1290

UNIVERSIDADE Ð COIMBRA

Manuel Francisco Silvério Carrilho Colaço

THE FOUR GLUON VERTEX FROM LATTICE QUANTUM CHROMODYNAMICS

Setembro de 2023

The Four Gluon Vertex from Lattice Quantum Chromodynamics

Manuel Francisco Silvério Carrilho Colaço

Supervisors:

Orlando Olavo Aragão Aleixo e Neves de Oliveira

Paulo de Jesus Henriques da Silva

A thesis submitted for the degree of Master in Physics

Coimbra, September 2023

Abstract

The interaction vertex functions of Quantum Chromodynamics are of fundamental importance in hadronic physics. These vertices control the interactions between quarks and gluons. Non-perturbative methods are required to evaluate these vertices in the low-energy scale.

Due to the convoluted tensor structure of four gluon vertex, non-perturbative methods face the challenge of extracting reliable data on this vertex. As such, it is poorly understood on the low-energy scale. Lattice Quantum Chromodynamics provide access to this non-perturbative regime. The following dissertation's work conducted exploratory research on employing this method to compute the four gluon vertex. This work chose the Landau gauge and did not consider the dynamics of quarks.

To implement an approach to determine the four gluon vertex on the lattice by computing its form factors, the vertex is constructed from first principles and in a set of chosen kinematic configurations that allow for the four gluon correlation function to depend solely on the four gluon vertex with its external legs contracted with the propagators. The form factors expressions can then be formulated by spanning this correlation function on a tensor basis and projecting the form factors by Lorentz-colour contractions of the correlation function with its basis elements. In principle, the tensor structure of the correlation function allows for a large number of possible tensor basis elements, but in the Landau gauge and this work's chosen kinematic configurations, the number of possible tensor basis elements is significantly reduced. This allows for practical access to lattice data from which the vertex form factors can be determined. The tensor basis considered in this work is incomplete, except for one of the chosen kinematic configurations.

The novel form factor data reported in this work achieved a reasonable signal-to-noise ratio and statistical errors, from which conclusions can be drawn. The data showed how, in general, the form factors' contribution to the vertex differed and how significant their dependence on the kinematic configuration was. Further improvements on this data can be accomplished by an increase in the lattice volume and size of the statistical ensemble generated by lattice simulations. Other realizations of Lattice Quantum Chromodynamics studies on the four gluon vertex can also be exercised by considering other vertex basis tensor elements and investigating different kinematic configurations.

Keywords: Lattice Quantum Chromodynamics, Non-perturbative Quantum Chromodynamics, Four gluon vertex , Quantum Chromodynamics, Gluon interaction

Resumo

As funções de vértice de interação da Cromodinâmica Quântica são de importância fundamental na física hadrónica. Estes vértices controlam as interações entre quarks e gluões. Para avaliar estes vértices na escala de baixas energias são necessários métodos não perturbativos.

Devido à estrutura tensorial convoluta do vértice de quatro gluões, os métodos não perturbativos enfrentam o desafio de extrair dados fiáveis sobre este vértice. Como tal, há uma ausência de conhecimento deste vértice na escala de baixas energias. A Cromodinâmica Quântica na rede permite aceder a este regime não perturbativo. No trabalho da dissertação que se segue foi conduzida uma investigação exploratória sobre o emprego deste método para calcular o vértice de quatro gluões. Neste trabalho foi escolhida a gauge de Landau e a dinâmica dos quarks não foi considerada.

Para implementar uma abordagem que permita determinar o vértice de quatro gluões na rede através do cálculo dos seus fatores de forma, o vértice é construído a partir de primeiros princípios e num conjunto de configurações cinemáticas escolhidas tal que permitem que a função de correlação de quatro gluões dependa apenas do vértice de quatro gluões com as suas pernas externas contraídas com os propagadores. As expressões dos fatores de forma podem então ser formuladas através da extensão desta função de correlação numa base tensorial e projetando os fatores de forma, através de contrações de cor e Lorentz da função de correlação com os seus elementos de base. Em princípio, a estrutura tensorial da função de correlação permite um grande número de elementos tensoriais da base, mas, na gauge de Landau e nas configurações cinemáticas escolhidas neste trabalho, o número de elementos de base tensoriais possíveis é significativamente reduzido. Isto permite um acesso prático a dados da rede a partir dos quais os fatores de forma dos vértices podem ser determinados. A base tensorial considerada neste trabalho é incompleta, exceto para uma das configurações cinemáticas escolhidas.

Os dados de fatores de forma relatados neste trabalho alcançaram uma razoável relação sinal-ruído e erros estatísticos, dos quais podem ser tiradas conclusões. Os dados mostraram como, em geral, as contribuições dos fatores de forma diferem entre si e o quão significativa é a sua dependência na configuração cinemática. Melhorias adicionais nestes dados podem ser conseguidas por um aumento no volume da rede e no tamanho da ensemble estatística gerada por simulações na rede. Outras realizações de estudos de Cromodinâmica Quântica de Rede no vértice de quatro gluões também podem ser exercidas considerando outros elementos tensoriais de base do vértice e investigando diferentes configurações cinemáticas.

Acknowledgments

I would like to express my gratitude for the guidance, support, and mentorship of my supervisors, Prof. Dr. Orlando Olavo Aragão Aleixo e Neves de Oliveira and Dr. Paulo de Jesus Henriques da Silva. Their insightful feedback and constructive criticism shaped the course of this thesis work, its writing process, and my academic development.

Additionally, I would not have been able to commit myself to this work if not for the help of my mother, sister and grandmother, to whom I am greatly in debt. Thank you for enduring my absence of mind.

Contents

List of Figures

Convention of Units and Notation

To simplify discussions, the following text will use Natural units, where the speed of light in vacuum c and the reduced Planck constant $\hbar$ are set to one,

$$c = \hbar = 1.$$

In this convention,

$$[\text{length}] = [\text{time}] = [\text{energy}]^{-1} = [\text{mass}]^{-1}.$$

The chosen Minkowski space-time metric signature is

$$g_{\mu\nu} = \text{diag}(+, -, -, -).$$

Einstein notation will be used, i.e. summation is assumed to any repeated indices within a term, whether or not each index occurs once as a superscript and once as a subscript, for example

$$\sum_{a,b} A^{a_1 \ldots a_n}_{b_1 \ldots b_m} B^{a_1 \ldots a_n}_{b_1 \ldots b_m} = A^{a_1 \ldots a_n}_{b_1 \ldots b_m} B^{a_1 \ldots a_n}_{b_1 \ldots b_m} = A^{b_1 \ldots b_m}_{a_1 \ldots a_n} B^{a_1 \ldots a_n}_{b_1 \ldots b_m}.$$

The chosen normalization convention for the $SU(N)$ generators in the fundamental representation (see Appendix A) will be

$$Tr(t^a t^b) = \frac{1}{2} \delta^{ab}.$$

Introduction

The Standard Model is a mathematical model of the fundamental structure of matter, consisting of the elementary particles and the forces that govern their interactions [42]. The weak, strong and electromagnetic forces govern these interactions.

Quantum Field Theory (QFT) is the theoretical framework of the Standard Model, and Quantum Chromodynamics (QCD) is the QFT belonging to the strongly interacting matter sector of the Standard Model [11]. QCD is formulated in terms of the elementary particles that constitute hadronic matter, quarks and gluons, where the latter are the force-carrying particles that mediate this interaction.

Even though the Standard Model has had remarkable success in explaining the outcome of particle physics experiments, it has shortcomings [28]. To demonstrate its deficiencies and search for physics beyond the Standard Model [36], it is necessary to understand it as well as possible.

At high energies (ultraviolet), QCD can be treated analytically with perturbation theory due to its asymptotic freedom [56]. This makes perturbative studies of QCD phenomena reliable at high energy scales [17]. However, there is no such analytical treatment of QCD at low energies (infrared), leading to invisible effects in the perturbative context. There are two prominent examples of low-energy phenomena. One is colour confinement [5], which describes the fact that no free quark or gluon has ever been observed, only their confinement within hadronic bound states, and the other is chiral symmetry breaking [50], which explains the observed masses of some mesons. The previous two mechanisms play a dominant role in determining the observable characteristics of QCD, and as such, there is a call for non-perturbative methods [34].

Two major *ab initio* approaches exist that can delve into the infrared scale of QCD, Lattice Quantum Chromodynamics [57] and Functional Methods [15,32], each with its advantages and disadvantages. Some examples of Functional Methods are the renormalization group [20], Dyson-Schwinger equations [5] and *n*-particle irreducible methods [8]. Although they set the stage for a non-perturbative exploration of QCD, they rely on truncating systems of equations by making some *ansatz*. This work follows the Lattice Quantum Chromodynamics approach, where the continuum Euclidean space-time is discretized and set on a finite volume lattice, allowing for numerical methods to be implemented. This method necessarily involves extrapolation between the lattice and continuum space-time, and, as such, the data found in this approach is subjected to errors originating from the continuum extrapolation.

Interaction vertex functions, also known as one-particle irreducible functions, control the interactions between quarks and gluons and are thus of prime theoretical interest for understanding hadronic physics. Several studies have put these vertices under the scrutiny of non-perturbative approaches [3, 4, 10, 13, 16, 18, 24, 29, 32, 35, 59], in the hopes of gaining insight into the aforementioned infrared regime of QCD. Of all elementary interaction vertices allowed by QCD, the four gluon vertex is the most poorly understood due to its intricate tensor structure, which considerably complicates the extraction of reliable, non-perturbative information.

Following the call for the non-perturbative study on the four gluon vertex, this work will conduct research by constructing this vertex from first principles and using Lattice QCD simulations to compute its form factors. Due to this vertex's previously stated convoluted tensor structure, this dissertation will be an explorative study bound by the choice of a set of kinematic configurations and tensor structures that allow for a practical extraction of data from Lattice QCD methods. Similar studies were conducted in [9, 12].

This dissertation is organized as follows. In Chapter 1, the formalism of Quantum Field Theory is outlined and reviewed, and with it, Quantum Chromodynamics is formulated, with particular emphasis on the concepts required for this work. In Chapter 2, the four gluon vertex is found from the four gluon Green functions in a specific kinematic configuration that allows isolating its contribution. With this, the vertex is spanned on a tensor basis, and expression for the form factors can be formulated by contractions of the Green function with the tensor basis elements. Chapter 3 starts by reviewing Lattice QFT, and with it, the gluon sector of Lattice QCD is devised. It then follows how to perform Lattice computations and extract data, particularly the lattice four gluon vertex data. This Chapter ends with a review of the different sources of errors affecting this data and how this work will approach them. Finally, Chapter 4 reports on this work's results.

1. The Basics of Quantum Chromo-dynamics

This chapter aims to review Quantum Chromodynamics and focus on the relevant concepts that will come into play in the following chapters. This chapter starts with a basic introduction to Quantum Field Theory. QCD is then formulated by first building the classical theory and then quantizing it. This subject's more complete and in-depth treatment can be found in [38, 45, 49, 51].

1.1 Quantum Field Theory and the Path Integral Approach

Quantum Field Theory is the most useful theoretical framework for studying elementary particle interactions, where the necessary information for experimental predictions is fully encapsulated in QFT's n-point Green functions. This can be seen in the LSZ reduction formula's formalism, which aims to compute S-matrix elements – the quantum mechanical transition amplitude between n asymptotic multi-particle states. Green functions are defined by the vacuum expectation value of the time-ordered products $\mathcal{T}$, of the generalized quantum mechanical field operators $\hat{\phi}_\alpha(x)$[1],

$$\langle 0| \mathcal{T}\{\hat{\phi}_{\alpha_1}(x_1)...\hat{\phi}_{\alpha_n}(x_n)\} |0\rangle \equiv \langle \hat{\phi}_{\alpha_1}(x_1)...\hat{\phi}_{\alpha_n}(x_n)\rangle \tag{1.1}$$

In the Minkowski space-time path-integral formalism [37], these functions are given by

$$\langle \hat{\phi}_{\alpha_1}(x_1)...\hat{\phi}_{\alpha_n}(x_n)\rangle = \frac{\int \mathcal{D}[\phi_\alpha]e^{iS[\phi_\alpha]}\phi_{\alpha_1}(x_1)...\phi_{\alpha_n}(x_n)}{\int \mathcal{D}[\phi_\alpha]e^{iS[\phi_\alpha]}}, \tag{1.2}$$

where on the r.h.s side, the fields are just regular functions, i.e. c-numbers.

$$\mathcal{D}[\phi_\alpha] = \prod_x \prod_\alpha d\phi_\alpha(x) \tag{1.3}$$

is the integration measure and

$$S[\phi_\alpha] = \int d^4x \, \mathcal{L}(\phi_\alpha(x), \partial_\mu \phi_\alpha^\mu(x)) \tag{1.4}$$

is the action – a functional of the field variables with $\mathcal{L}(\phi_\alpha(x), \partial_\mu \phi_\alpha^\mu(x))$ being the classical Lagrangian density. The Green functions are evaluated by a functional integration over all the possible

---

[1]α is a generalized indexation of possibly different fields and their respective internal degrees of freedom.

paths in the fields configuration space, starting and ending at vacuum, i.e. $\phi_\alpha(x) = 0$, with $S[\phi_\alpha]$ acting as a weight for every each path. It then follows that the Lagrangian density, as a function of the classical fields, defines the quantum theory's dynamics by determining the exponent in the path integral and a classical theory is quantized.

Note that it has been assumed that there are infinitely many interacting degrees of freedom. Practically, this means that when computing the Green functions, one has to consider arbitrarily short and long distances or equivalently high and low energies, respectively [47]. In perturbation theory, this leads to the divergent loop integrals [41], which can be made finite by introducing a regulator in the loop integrals such that these become convergent. This regulator introduces a scale into the theory. The regulator-dependent parts can then be separated from the independent ones and seen as the source of divergence when the regulator is adequately removed. Doing this allows one to identify, isolate and remove these infinities by renormalizing the theory, i.e. redefining the theory's parameters, void of any direct physical meaning, given as the bare masses, coupling constants and field strengths such that these infinities get removed. In lattice QCD (Chapter 3), this scale ambiguity is dealt with by defining the theory on a discrete space-time lattice with a finite lattice spacing and volume that regularizes the theory, i.e. rendering it finite in both the infrared and ultraviolet.

1.1.1 Quantum Effective Action

Computing the Green functions by exact evaluation in the continuum space-time path integral (1.2) is not a practical possibility. In Chapter 3, we will see how this integration can be approximated with the formalism of lattice QCD. Still, in continuum space-time, one way to define the Green functions is by using the generating functional

$$Z[J_\alpha] = \int \mathcal{D}[\phi] e^{i \int d^4x \left\{ \mathcal{L}(\phi_\alpha(x), \partial_\mu \phi_\alpha^\mu(x)) - J_\alpha(x)\phi_\alpha(x) \right\}}. \tag{1.5}$$

Here, $Z[J_\alpha]$ is the generating functional depending on the auxiliary source field $J_\alpha(x)$ of the $\phi_\alpha(x)$ classical field functions. The Green functions are then computed by the functional differentiation

$$\langle \hat{\phi}_{\alpha_1}(x_1)...\hat{\phi}_{\alpha_n}(x_n) \rangle = i^n \frac{1}{Z[J_\alpha]} \frac{\delta^n Z[J_\alpha]}{\delta J_{\alpha_1}(x_1)...\delta J_{\alpha_n}(x_n)} \bigg|_{J_\alpha=0}. \tag{1.6}$$

However, there are other functionals from which one can build the Green functions by functional differentiation. Defining the quantum effective action as

$$\Gamma[\Phi_\alpha] = W[J_\alpha] + \int d^4x \, \Phi_\alpha(x) J_\alpha(x) \tag{1.7}$$

with

$$W[J_\alpha] = -i \ln Z[J_\alpha] \tag{1.8}$$

and

$$\Phi_\alpha(x) = -\frac{\delta W[J_\alpha]}{\delta J_\alpha(x)} = \frac{1}{Z[J_\alpha]} \frac{i\delta}{\delta J(x)_\alpha} Z[J_\alpha] \equiv \frac{\langle \hat{\phi}_\alpha(x) \rangle_J}{\langle 0|0 \rangle_J}, \tag{1.9}$$

the vacuum expectation value of the field ϕ_α in the presence of the source field J_α, which vanishes when $J_\alpha = 0$.

4

In a perturbative evaluation of the path-integral, which entails the use of Feynman diagrams [60], it is seen that the Green functions generated by the generating functional (1.6) contain disconnected graphs and connected graphs. The former graphs do not contribute to the S-matrix. The latter contains redundant information in the form of external propagators, which are common to all graphs, and one-particle reducible graphs that can be separated by removing a propagator that connects the two. The quantum effective action is the generator of the one-particle irreducible Green functions, which eliminate redundancies and encode only the relevant information for calculations.

From the effective action (1.7), it follows that

$$J_\alpha(x) = \frac{\delta\Gamma[\Phi_\alpha]}{\delta\Phi_\alpha(x)}, \tag{1.10}$$

which can be used with (1.7) and (1.9) to give the orthogonality relation

$$\int d^4y \, \frac{\delta^2 W[J_\alpha]}{\delta J_{\alpha_1}(x)\delta J_{\alpha_2}(y)} \frac{\delta^2\Gamma[\Phi_\alpha]}{\delta\Phi_{\alpha_2}(y)\delta\Phi_{\alpha_3}(z)} = -\delta_{\alpha_1\alpha_3}(x-z). \tag{1.11}$$

From this expression we see that

$$-\left[\frac{\delta^2\Gamma[\Phi_\alpha]}{\delta\Phi_{\alpha_2}(x)\delta\Phi_{\alpha_3}(y)}\right]^{-1} = \frac{\delta^2 W[J_\alpha]}{\delta J_{\alpha_2}(x)\delta J_{\alpha_3}(y)} \equiv D^{xy}_{\alpha_1\alpha_2}[\Phi], \tag{1.12}$$

with $D^{xy}_{\alpha_1\alpha_2}[\Phi]$ being the $\phi_\alpha(x)$ field propagator in the presence of a source $J_\alpha(x)$ and

$$-iD^{xy}_{\alpha_1\alpha_2}[\Phi]\Big|_{J_\alpha=0} = \langle\hat{\phi}_{\alpha_1}(x)\hat{\phi}_{\alpha_2}(y)\rangle \equiv D_{\alpha_1\alpha_2}(x,y). \tag{1.13}$$

Using these definitions on the expression that finds the n-point Green functions from the generating functional (1.6), and after some algebra, we can find the identity

$$\langle\hat{\phi}_{\alpha_1}(x_1)...\hat{\phi}_{\alpha_n}(x_n)\rangle = \left[\Phi_\alpha(x) + \int d^4y \, D^{xy}_\alpha[\Phi_\alpha]\frac{i\delta}{\delta\Phi_\alpha(y)}\right]^n\Bigg|_{J_\alpha=0} \tag{1.14}$$

which is the relation that we were after. This allows one to find the n-point Green functions from functional differentiation of the quantum effective action, i.e., the one-particle irreducible graphs, also known as the n-point vertex functions:

$$\frac{\delta^n\Gamma[\Phi_\alpha]}{\delta\Phi_{\alpha_1}(x_1)...\delta\Phi_{\alpha_n}(x_n)}\Bigg|_{J_\alpha=0} \equiv \Gamma_{\alpha_1...\alpha_n}(x_1,...,x_n). \tag{1.15}$$

1.2 Formulating Quantum Chromodynamics

Quantum Chromodynamics is the QFT of strong force interactions associated with the colour-charged[2] elementary particles quarks and gluons. There are three types of colour that, by convention, are labelled red, green, or blue. Such a theory needs to be symmetric under gauge transformations of these colour charge degrees of freedom[3].

---

[2]Historically, colour charge quantum number was introduced so that the observed ground state of hadrons would agree with the spin-statistics theorem.

[3]The colour labels that are given to QCD's elementary particles are redundant, only the relationship between these degrees of freedom is relevant.

Following the concepts introduced earlier, formulating this colour gauge theory requires the expression for the Lagrangian density. For this, one can start by writing the quark and anti-quark fields as

$$\psi_{\alpha,f,j}(x), \quad \psi^{\dagger}_{\alpha,f,c}(x)\gamma^0 \equiv \overline{\psi}_{\alpha,f,j}(x), \tag{1.16}$$

respectively. They are Dirac spinors, indexed by α, with f and j indexing the six flavour and three colour degrees of freedom, respectively. The former two indices are irrelevant in the following discussion and will be suppressed. The Dirac Lagrangian density that provides the dynamical content of these fields can be written as

$$\mathcal{L}_{Dirac} = \overline{\psi}_j(x)\left(i\gamma^{\mu}\partial_{\mu} - m\right)\psi_j(x), \tag{1.17}$$

where the flavour diagonal matrix m gives the different quark flavour bare masses.

Due to the complex-valued triplet colour structure of these fields, colour gauge symmetry is realized by imposing the symmetry of the previous expression under $SU(3)$ group local transformations in the fundamental representation,

$$\psi_i(x) \longrightarrow V_{ij}(x)\psi_j(x), \tag{1.18}$$

and anti-fundamental representation,

$$\psi^{\dagger}_i(x) \longrightarrow \psi^{\dagger}_j(x)V^{\dagger}_{ij}(x), \tag{1.19}$$

with

$$V_{ij}(x) \equiv \exp[i\theta^a(x)t^a_{ij}], \tag{1.20}$$

where t^a are the eight generators of $SU(3)$ in the fundamental representation and $\theta^a(x)$ are real numbers that parameterize the transformation.

The derivative term in $\mathcal{L}_{Dirac}$ (1.17) requires evaluation of $\psi(x)$ at two different points in space-time separated by an infinitesimal distance, resulting in this expression not being invariant under the transformations (1.18) and (1.19). To deal with the lack of gauge symmetry, we introduce the link variable $U(x,y)$, defined by the path-ordered exponential[4]

$$U(x,y) = \mathcal{P}\{\exp\left(ig\int_x^y dl^{\mu}A_{\mu}(z)\right)\}, \tag{1.21}$$

where the matrix-valued gauge field A_{μ} will be defined later on, and g is this field's bare coupling constant. The link variable can be set to follow the gauge transformation in the adjoint representation

$$U(x,y) \longrightarrow V(x)U(x,y)V^{\dagger}(y). \tag{1.22}$$

With this, we can now define the covariant derivative D_{μ} as

$$D_{\mu}\psi(x) \equiv \lim_{\epsilon \to \infty} \frac{1}{\epsilon}[U(x,x+\epsilon)\psi(x+\epsilon) - \psi(x)], \tag{1.23}$$

---

[4]The path-ordering ensures that exponential matrix definition as a power series is still valid even if they are non-commutative.

Following the transformations (1.18) and (1.22) leads to this expression having the gauge transformation

$$D_\mu \psi(x) \longrightarrow V(x) D_\mu \psi(x). \tag{1.24}$$

The derivative term of (1.17) with ∂_μ replaced by D_μ is now invariant under this gauge transformation. To now find an expression for D_μ we can write the Taylor Series expansion,

$$U(x, x + \epsilon) = I_3 - ig\epsilon^\mu A_\mu(x) + \mathcal{O}(\epsilon^2), \tag{1.25}$$

Substituting this expression in (1.23), we find

$$D_\mu = \partial_\mu - igA_\mu(x), \tag{1.26}$$

The transformation of $A_\mu(x)$ can be readily found by inserting (1.25) in (1.23),

$$A_\mu(x) \longrightarrow V(x) A_\mu(x) V^\dagger(x) - \frac{i}{g} [\partial_\mu V(x)] V^\dagger(x). \tag{1.27}$$

From this, we see that $A_\mu(x)$ transforms in the adjoint representation and so can be written with the generators in the fundamental representation as

$$A_\mu(x) = A_\mu^a(x) t^a. \tag{1.28}$$

This newly introduced gauge field can be then be identified as the eight different gluon fields[5]. Promoting it to a dynamical field requires a gauge invariant kinetic term. This can be found by inspection of the gauge field transformation (1.27) on

$$F_{\mu\nu}(x) = \frac{i}{g} [D_\mu, D_\nu], \tag{1.29}$$

with $F_{\mu\nu}(x)$ the field-strength tensor, from which it is seen to transform as

$$F_{\mu\nu}(x) \longrightarrow V(x) F_{\mu\nu}(x) V^\dagger(x). \tag{1.30}$$

Like (1.28), the field-strength tensor can be defined in the adjoint representation,

$$F_{\mu\nu}(x) = F_{\mu\nu}^a t^a. \tag{1.31}$$

and the required gauge invariant kinetic term can be written as

$$-\frac{1}{4} F_{\mu\nu}^a F^{a\mu\nu} = -\frac{1}{2} Tr(F_{\mu\nu} F^{\mu\nu}), \tag{1.32}$$

with,

$$F_{\mu\nu}^a(x) = \partial_\mu A_\nu^a - \partial_\nu A_\mu^a + g f^{abc} A_\mu^b A_\nu^c. \tag{1.33}$$

---

[5]Gluons's colour degrees of freedom (red, anti-red, green, anti-green, blue and anti-blue) can be found by noting that the $SU(3)$ fundamental representation, R_f, is spanned by the quark colour triplet (eq.1.18) and anti-fundamental representation, $\overline{R_f}$, spanned by the anti-quark colour triplet (eq.1.19). These representations can be used to write the adjoint representation, R_{adj}, in the tensor product $R_f \otimes \overline{R}_f = R_{adj} \otimes 1$ by using [25], therefore preserving the quark and anti-quark colour organization scheme in the adjoint representation.

The Dirac Lagrangian (1.17) and the expressions resulting from demanding gauge invariance, (1.26) and (1.32), now allow the writing of the colour charge gauge symmetric Lagrangian density,

$$\mathcal{L}_{QCD} = -\frac{1}{2} Tr(F_{\mu\nu} F^{\mu\nu}) + \overline{\psi} \left(i\gamma^\mu D_\mu - m \right) \psi. \tag{1.34}$$

The first term is also known as the $SU(3)$ Yang-Mills theory's Lagrangian,

$$\mathcal{L}_{\text{YM}} = -\frac{1}{2} Tr(F_{\mu\nu} F^{\mu\nu}). \tag{1.35}$$

As this work aims to investigate the four gluon vertex, the previous expression is of special importance, as will be seen in Chapter 3.

1.2.1 Quantization and Gauge Fixing

The transformation property of the gauge fields (1.27) introduced an infinite number of redundant degrees of freedom. With this transformation, $V(x)$ relates gauge equivalent fields in what is called a gauge orbit. These redundant degrees of freedom describe the same physics, and with their presence, a naive quantization of the classical field theory described in the previous section leads to integrations of the form

$$\int \mathcal{D}[A] e^{iS[A]}. \tag{1.36}$$

Here, $\mathcal{D}[A]$ takes into account the infinite number of gauge fields in a given gauge orbit related by the gauge transformation (1.27). Such a contribution will lead to the divergence of the integration over the gauge orbit, resulting in an ill-defined generating functional (1.2). This shows the need to adequately discard the gauge orbit redundant degrees of freedom, which is the scope of the Faddeev–Popov procedure [62]. The outcome of this method is

$$\int \mathcal{D}[A] e^{iS[A]} = \int \mathcal{D}[\theta] \int \mathcal{D}[A] e^{iS[A]} \det \left(\frac{\delta f^a[A]}{\delta \theta^b} \right) \bigg|_{\theta=0} \exp \left(\frac{-i}{2\xi} \int d^4x \, f^a[A]^2 \right), \tag{1.37}$$

where on the r.h.s, the first integration is over the gauge orbit, amounting to a factor that can be formally cancelled in the theory's Green functions (1.2). The functional $f^a[A]$ is a gauge fixing condition verifying $f^a[A] = 0$, and it has been assumed that this constraint is ideal, i.e. only one $A^a(x)$ in the gauge orbit integration satisfies this. Generally, this is not the case, and one has to deal with Gribov Ambiguity [30]. The real number ξ is a parameter that determines a choice of gauge.

Gauge fixing results in the breaking of gauge symmetry, leading to gauge-dependent Green functions. For the rest of this dissertation, the Landau gauge fixing condition

$$f^a[A^\theta] = \partial^\mu A_\mu^a = 0 \tag{1.38}$$

is chosen. The outcome of experiments is gauge-independent. To compute gauge unconstrained observables, the response of the gauge-dependent Green functions with the change of gauge conditions is needed, such that one can relate Green functions defined with different gauges. This is accomplished by the Slavnov-Taylor identities [53].

2. Four Gluon Vertex

The main goal of this dissertation's work is to compute the four gluon vertex in the Landau Gauge. This chapter is dedicated to finding how this can be done from what is accessible in Lattice QCD simulations (see Chapter 3). This introduces the necessity of expressing the Green functions in terms of their form factors, which is done by exploiting the tensor structure of the Green functions. As will be seen, this is a challenging task, so one must resort to restrictions stemming from theoretical arguments and computation capabilities. In what follows, the fermionic sector of QCD is neglected.

2.1 Green Functions in a Tensor Basis

An n-point gluon Green function ($2 \leq n \leq 4$) in momentum-space[6] has $n-1$ independent external momenta. It can be spanned in the assumed to be complete N-dimensional tensor basis, with N depending on the type of Green function, by using N-independent tensor structures $\{t^{(i)}\}$,

$$\langle A^{a_1}_{\mu_1}(p_1)...A^{a_n}_{\mu_n}(p_n) \rangle = \sum_{i=1}^{N} \left(F^{(i)}(p_1^2, ..., p_n^2, p_1 \cdot p_2, ...)t^{(i)a_1...a_n}_{\mu_1...\mu_n}(p_1, ..., p_n) \right) (2\pi)^4 \delta(p_1 + ... + p_n), \tag{2.1}$$

where F^i are form factors that encapsulate the physical content of the Green functions. They depend on all possible Lorentz invariant momentum variables such that the Green functions comply with Bose-symmetry.

The available Lorentz and colour building blocks of such a basis are $\{g_{\mu\nu}, p_\mu\}$ and $\{\delta^{ab}, f^{abc}, d^{abc}\}$, respectively. These can then be combined in every possible way that complies with the constraints of the Green functions, where p stands for all independent momenta.

The gluon propagator, in momentum space, is given by

$$\langle A^a_\mu(p_1)A^b_\nu(p_2) \rangle = D^{ab}_{\mu\nu}(p) (2\pi)^4 \delta(p_1 + p_2). \tag{2.2}$$

Its tensor structure is constrained by the Slavnov-Taylor identity, which in the Landau gauge reads

$$p^\mu p^\nu D^{ab}_{\mu\nu}(p) = 0. \tag{2.3}$$

---

[6]The momentum-space Green functions is found by Fourier transforming the space-time Green functions, hence the appearance of the Dirac-delta function and the $(2\pi)^4$ factor.

The only available rank-2 tensors for building this expression are δ^{ab}, $g_{\mu\nu}$ and $p_\mu p_\nu$[7]. These structures and the previous identity fix the simple tensor structure of the gluon propagator to be

$$D_{\mu\nu}^{ab}(p) = D(p^2)\delta^{ab}P_{\mu\nu}(p), \tag{2.4}$$

where

$$P_{\mu\nu}(p) = \left(g_{\mu\nu} - n\frac{p_\mu p_\nu}{p^2}\right) \tag{2.5}$$

with $p^\mu P_{\mu\nu}(p) = 0$ the momentum-orthogonal projector and $n = 0$ if $p = 0$ and $n = 1$ if $p \neq 0$. Using this tensor decomposition, the form factor can be projected when multiplying both sides of the propagator (2.2) by $\delta^{ab}g^{\mu\nu}$, giving

$$\delta(p_1 + p_2)\,D(p^2) = \frac{\langle Tr\,[A_\mu(p_1)A_\mu(p_2)]\rangle}{(2\pi)^4\,(16 - 4n)} \tag{2.6}$$

On the other hand, the three independent external momenta and Lorentz-colour tensor structure of the four gluon Green function make it extremely rich, complex and cumbersome to compute its form factors since it allows a large range of Lorentz-colour rank-4 linearly independent basis elements:

$$\langle A_\mu^a(p_1)A_\nu^b(p_2)A_\eta^c(p_3)A_\zeta^d(p_4)\rangle = \sum_{i=1}^{N}\left(F^{(i)}t_{\mu\nu\eta\zeta}^{(i)abcd}(p_1,p_2,p_3,p_4)\right)(2\pi)^4\,\delta(p_1 + p_2 + p_3 + p_4), \tag{2.7}$$

with

$$F^{(i)} \equiv F^{(i)}\left(p_1^2 + ... + p_4^2, (p_1 \cdot p_2) + (p_1 \cdot p_3) + (p_1 \cdot p_4) + (p_2 \cdot p_3) + (p_2 \cdot p_4) + (p_3 \cdot p_4)\right), \tag{2.8}$$

the Bose-symmetric form factor, with this being the only possible momenta variable dependence.

As stated in this chapter's introduction, this work's goal is to find the four gluon vertex - i.e. computing its form factors. To do so, one needs to isolate these from the Green functions form factors (2.7).

2.2   Isolating the Vertex

As will be seen in Chapter 3, Lattice QCD simulations only access the Green functions. The lattice evaluation of vertices can then only be achieved if the Green functions are decomposed in terms of vertex functions. To find the four gluon vertex, one can start by using expression (1.14) to express the 4-point gluon Green functions[8] as a function of functional derivatives of the quantum effective action. Doing so, and Fourier transforming into momentum-space, we get

$$\langle A_\mu^a(p_1)A_\nu^b(p_2)A_\sigma^c(p_3)A_\zeta^d(p_4)\rangle = G_{\mu\nu\sigma\zeta}^{abcd}(p_1,p_2,p_3,p_4)\,(2\pi)^4\,\delta(p_1 + p_2 + p_3 + p_4), \tag{2.9}$$

---

[7]If $p = 0$, $p_\mu p_\nu$ is discarded.

[8]From now on, the field operator circumflex notation will be omitted.

Figure 2.1: Diagrammatic representation of expression (2.10), i.e. the four gluon Green functions, denoted the black circle, which decomposed in terms of the gluon propagator, as well as the three and four vertices, all denoted here by the shaded circles. Lorentz, colour and momenta indices are omitted.

with

$$
\begin{aligned}
G_{\mu\nu\eta\zeta}^{abcd}(p_1, p_2, p_3, p_4) =\ & D_{\mu\mu'}^{aa'}(p_1) D_{\nu\nu'}^{bb'}(p_2) D_{\eta\eta'}^{cc'}(p_3) D_{\zeta\zeta'}^{dd'}(p_4) \Gamma_{a'b'c'd'}^{\mu'\nu'\eta'\zeta'}(p_1, p_2, p_3, p_4) \\
& - i D_{\mu\tilde{\mu}}^{a\tilde{a}}(p_1) D_{\nu\nu'}^{bb'}(p_2) \Gamma_{\tilde{a}b'\tilde{b}'}^{\tilde{\mu}\nu'\tilde{\nu}'}(p_1, p_2, p_1 + p_2) \\
& \times D_{\tilde{\nu}'\tilde{\nu}}^{\tilde{b}'\tilde{b}}(p_1 + p_2) \Gamma_{\tilde{b}c'd'}^{\tilde{\nu}\eta'\zeta'}(p_3, p_4, p_3 + p_4) D_{\eta\eta'}^{cc'}(p_3) D_{\zeta\zeta'}^{dd'}(p_4) \\
& + D_{\mu\nu}^{ab}(p_1) \delta(p_1 + p_2) D_{\eta\zeta}^{cd}(p_4) \delta(p_3 + p_4) \\
& + \text{cyclic permutations.}
\end{aligned}
\tag{2.10}
$$

This expression is diagrammatically represented in Figure 2.1. In the following chapter, it will be seen that, in lattice QCD, one only has access to $G_{\mu\nu\eta\zeta}^{abcd}(p_1, p_2, p_3, p_4)$. To compute the four gluon vertex form factors, one could, in principle, consider every term in the last expression and then subtract the contribution of the three 3-vertices and disconnected propagators terms from the four gluon vertex, but in the next chapter, we will see that this would heavily hinder the lattice simulations. One can remove these troublesome term contributions with a suitable choice of independent external momenta kinematics. Firstly, the disconnected propagators can be removed if any two external propagators i and j are such that $p_i + p_j \neq 0$. In Appendix B, the remaining 3-vertex terms can also be seen to vanish by choosing a kinematic configuration with proportional external momentum, i.e. when

$$
p_1 = c_1 p, \quad p_2 = c_2 p, \quad p_3 = c_3 p, \quad p_4 = (-c_1 - c_2 - c_3)\, p.
\tag{2.11}
$$

11

With this, we finally have:

$$\langle A_\mu^a(p_1)A_\nu^b(p_2)A_\eta^c(p_3)A_\zeta^d(p_4)\rangle = D_{\mu\mu'}^{aa'}(p_1)D_{\nu\nu'}^{bb'}(p_2)D_{\eta\eta'}^{cc'}(p_3)D_{\zeta\zeta'}^{dd'}(p_4)$$
$$\times\, \Gamma_{a'b'c'd'}^{\mu'\nu'\eta'\zeta'}(p_1,p_2,p_3,p_4)(2\pi)^4\delta(p_1+p_2+p_3+p_4), \tag{2.12}$$

where the four gluon vertex term has been isolated.

2.3 Computing the Vertex Form Factors

2.3.1 Tensor basis

Spanning the four gluon vertex in a suitable tensor basis enables expressing its form factors. In [9, 12, 23, 29, 33], discussions have been made on the possible tensor structure of the four gluon vertex basis, composed by combinations of members of the rank-4 Lorentz-colour tensors sets: $\{g_{\mu\nu}g_{\eta\zeta}, g_{\mu\nu}p_\eta p_\zeta, p_\mu p_\nu p_\eta p_\zeta\}$ and $\{\delta^{ab}\delta^{cd}, f^{abr}f^{cdr}, f^{abr}d^{cdr}, d^{abr}d^{cdr}\}$. Due to the vast amount of possible basis tensors shown in these studies, one is forced to adopt some restriction to a smaller subset of basis elements. One major simplification is made with the previously chosen kinematics (2.11) by noting that vertex basis tensors with four-momenta structure vanish when contracted with the momenta-orthogonal projectors (2.5), hence leaving only the possible Lorentz rank-4 tensor $\{g_{\mu\nu}g_{\eta\zeta}\}$ as building blocks that contributes to the Green function tensor structure.

In this work, from the remaining possible basis structure, to build such a basis, we first consider the tree level four gluon vertex,

$$t_{abcd}^{(1)\mu\nu\eta\zeta} = f_{abr}f_{cdr}(g^{\mu\zeta}g^{\nu\eta} - g^{\mu\eta}g^{\nu\zeta}) + f_{acr}f_{bdr}(g^{\mu\nu}g^{\zeta\eta} - g^{\mu\eta}g^{\nu\zeta})$$
$$+ f_{adr}f_{bcr}(g^{\mu\nu}g^{\eta\zeta} - g^{\mu\zeta}g^{\nu\eta}). \tag{2.13}$$

This is the leading order contribution to the four gluons interaction in perturbation theory, which surely contributes to the high momentum limit of the vertex basis built here.

A near-identical structure can be found by replacing the anti-symmetric f_{abc} with the symmetric d_{abc}, symmetrizing the Lorentz structures, such that Bose-Symmetry is preserved. Such a basis element is:

$$\tilde{t}_{abcd}^{(1)\mu\nu\eta\zeta} = d_{abr}d_{cdr}(g^{\mu\eta}g^{\nu\zeta} + g^{\mu\zeta}g^{\nu\eta}) + d_{acr}d_{bdr}(g^{\mu\zeta}g^{\nu\eta} + g^{\mu\nu}g^{\eta\zeta})$$
$$+ d_{adr}d_{bcr}(g^{\mu\nu}g^{\eta\zeta} + g^{\mu\eta}g^{\nu\zeta}). \tag{2.14}$$

The last structure that shall be considered here is

$$t_{abcd}^{(2)\mu\nu\eta\zeta} = (g^{\zeta\eta}g^{\mu\nu} + g^{\zeta\nu}g^{\mu\eta} + g^{\zeta\mu}g^{\nu\eta})(\delta^{ab}\delta^{cd} + \delta^{ac}\delta^{bd} + \delta^{ad}\delta^{bc}), \tag{2.15}$$

which was also studied as a basis structure in [9].

These tensors do not form an orthogonal basis, as can be seen in the Lortenz-colour contractions, denoted here by $\cdot$,

$$t^{(1)} \cdot t^{(2)} = 0$$
$$\tilde{t}^{(1)} \cdot t^{(2)} \neq 0 \tag{2.16}$$
$$\tilde{t}^{(1)} \cdot t^{(1)} \neq 0.$$

12

But from this, one also sees that a new tensor can be defined,

$$t^{(3)} \equiv \frac{1}{\tilde{t}^{(1)} \cdot t^{(1)}} \tilde{t}^{(1)} - \frac{1}{t^{(1)} \cdot t^{(1)}} t^{(1)} - \frac{\tilde{t}^{(1)} \cdot t^{(2)}}{\left(t^{(2)} \cdot t^{(2)}\right)\left(\tilde{t}^{(1)} \cdot t^{(1)}\right)} t^{(2)}, \tag{2.17}$$

such that $\{t^{(1)}, t^{(2)}, t^{(3)}\}$ is an orthogonal tensor basis, following the relation

$$t^{(i)} \cdot t^{(j)} = N_j \delta^{ij}, \tag{2.18}$$

where

$$N_1 = t^{(1)} \cdot t^{(1)}, \quad N_2 = t^{(2)} \cdot t^{(2)}, \quad N_3 = t^{(3)} \cdot t^{(3)}. \tag{2.19}$$

2.3.2 Form Factors

The four gluon vertex may now be written on this basis,

$$\Gamma^{\mu'\nu'\eta'\zeta'}_{a'b'c'd'}(p^2) = \bar{F}^{(1)}(p^2) t^{(0)\mu'\nu'\eta'\zeta'}_{a'b'c'd'} + \bar{F}^{(2)}(p^2) t^{(2)\mu'\nu'\eta'\zeta'}_{a'b'c'd'} + \bar{F}^{(3)}(p^2) t^{(3)\mu'\nu'\eta'\zeta'}_{a'b'c'd'} + \ldots, \tag{2.20}$$

where the vertex form factors momenta dependence follow (2.8) and the kinematic configuration (2.11), with the ellipsis expressing the fact that this is not necessarily a complete basis. This vertex can now be inserted in the four gluon Green function expression found in (2.24),

$$\begin{aligned}
\langle A^a_\mu(p_1) A^b_\nu(p_2) A^c_\eta(p_3) A^d_\zeta(p_4) \rangle = &\; D^{aa'}_{\mu\mu'}(p_1) D^{bb'}_{\nu\nu'}(p_2) D^{cc'}_{\eta\eta'}(p_3) D^{dd'}_{\zeta\zeta'}(p_4) \\
&\times \left(\bar{F}^{(1)}(p^2) t^{(0)\mu'\nu'\eta'\zeta'}_{a'b'c'd'} + \bar{F}^{(2)}(p^2) t^{(2)\mu'\nu'\eta'\zeta'}_{a'b'c'd'} + \bar{F}^{(3)}(p^2) t^{(3)\mu'\nu'\eta'\zeta'}_{a'b'c'd'} + \ldots \right) \\
&\times (2\pi)^4 \delta(p_1 + p_2 + p_3 + p_4).
\end{aligned} \tag{2.21}$$

Similarly to what was done in the gluon propagator (2.6), the four gluon Green function form factors, defined in (2.7), can be found by the projection

$$\delta(p_1 + p_2 + p_3 + p_4) F^{(i)}(p^2) = \frac{1}{(2\pi)^4} t^{(i)abcd}_{\mu'\nu'\eta'\zeta'} g^{\mu'\mu} g^{\nu'\nu} g^{\eta'\eta} g^{\zeta'\zeta} \langle A^a_\mu(p_1) A^b_\nu(p_2) A^c_\eta(p_3) A^d_\zeta(p_4) \rangle. \tag{2.22}$$

In the next chapter, we will see that this expression can be computed in the lattice formalism. The four gluon vertex form factors can then be found with

$$\bar{F}^{(i)}(p^2) = \frac{F^{(i)}}{g^{\mu'\mu} g^{\nu'\nu} g^{\eta'\eta} g^{\zeta'\zeta} D^{aa'}_{\mu\mu'}(p_1) D^{bb'}_{\nu\nu'}(p_2) D^{cc'}_{\eta\eta'}(p_3) D^{dd'}_{\zeta\zeta'}(p_4) t^{(i)abcd}_{\mu'\nu'\eta'\zeta'} t^{(i)\mu'\nu'\eta'\zeta'}_{a'b'c'd'}}. \tag{2.23}$$

The reader is again reminded that these are found on a basis that is not necessarily complete. Therefore, the form factors found here may contain contributions from form factors associated with basis elements that are not considered. Appendix B makes these expressions explicit for the three $t^{(i)}$ and kinematic configurations chosen in this study. The latter are

$$\begin{aligned}
p_1 &= p, & p_2 &= p, & p_3 &= p, & p_4 &= -3p & (p, p, p, -3p), \\
p_1 &= 0, & p_2 &= p, & p_3 &= p, & p_4 &= -2p & (0, p, p, -2p), \\
p_1 &= 0, & p_2 &= p, & p_3 &= 2p, & p_4 &= -3p & (0, p, 2p, -3p).
\end{aligned} \tag{2.24}$$

Of utmost importance is configuration $(p, p, p, -3p)$, where in [9], it was shown that this reduced the number of different possible form factors to three, ensuring that our chosen tensor basis is complete.

13

3. Lattice Quantum Chromodynamics

This chapter follows the structure of Chapter 1, providing a review of what lattice QCD is and how to perform lattice simulation on a computer, applied to the determination of the four gluon functions. A detailed introduction to the formulation of a QFT on a lattice with applications to QCD can be found in [26, 48, 54].

3.1   The Path Integral in Euclidean Space-Time

In the path-integral approach to QCD, the computation of the Green functions requires integrating over the field configuration space. This calls for a numerical computation that is especially difficult due to the oscillating behaviour of e^{iS}. The convergence problems due to the nature of the integrand can be improved by changing from Minkowski to Euclidean space-time by rotating the time coordinate to the imaginary axis $t \longrightarrow it$, known as Wick rotation. It can be seen that this analytic continuation leads to

$$e^{iS} \xrightarrow[t \longrightarrow it]{} e^{-S_E}, \tag{3.1}$$

where S_E is the Euclidean action. This removes the oscillating behaviour in the path integral and allows a convergent exponential decay if the action is real and bounded from below. See [44] for a proper formulation of how to link Euclidean and Minkowski space-time field theory.

We can now write the Euclidean space-time path integral and Green functions as

$$\langle \hat{\phi}_{\alpha_1}(x_1)...\hat{\phi}_{\alpha_n}(x_n) \rangle_E = \frac{\int \mathcal{D}[\phi] e^{-S_E[\phi]} \phi_{\alpha_1}(x_1)...\phi_{\alpha_n}(x_n)}{\int \mathcal{D}[\phi] e^{-S_E[\phi]}}, \tag{3.2}$$

where we see that this expression can be read as a statistical ensemble average, with a Boltzmann distribution given by e^{-S_E}. Therefore, the Euclidean Green functions can now be interpreted as correlation functions, and one can use statistical physics methods to compute the correlation functions, such as Monte Carlo simulations [39]. The lattice formulation developed in this chapter will allow the practical implementation of this numerical method by constraining the previous integrations to a discretized space-time in a finite volume. Henceforth, we will work in the Euclidean space-time and remove $_E$ to simplify notation.

3.2 Lattice Quantum Field Theory

The discretization of space-time on a lattice can be written as

$$x_\mu = an_\mu, \quad n_\mu \in \mathbb{Z}^4 \tag{3.3}$$

where a is the lattice spacing. In the commonly used restriction of x_μ to a hypercubic lattice of volume $V = L^4$, we have

$$n_\mu \in \{0, 1, ..., N-1\}_\mu \tag{3.4}$$

and $L = aN$. With this, space-time is defined in a finite volume V and restricted to a finite set of points separated by the lattice spacing a.

Two immediate consequences can be found by inspecting the restriction of the continuum Fourier transform,

$$\phi(x) = \int \frac{d^4p}{(2\pi)^4} \tilde{\phi}(p) e^{ip_\mu x_\mu}, \tag{3.5}$$

to the discrete space-time domain of field $\phi(x)$. Due to the finite volume of the hypercube (3.4), periodic boundary conditions can be imposed,

$$\phi(x_\mu) = \phi(x_\mu + aN\hat{\mu}), \tag{3.6}$$

where $\hat{\mu}$ is the unit lattice vector in the direction μ. It follows that

$$
\begin{aligned}
\phi(x) &= \int \frac{d^4p}{(2\pi)^4} \tilde{\phi}(p) e^{ip_\mu x_\mu} = \int \frac{d^4p}{(2\pi)^4} \tilde{\phi}(p) e^{ip_\mu(x_\mu + aN\hat{\mu})} \\
&= \int \frac{d^4p}{(2\pi)^4} \tilde{\phi}(p) e^{i(p_\mu x_\mu + aN p_\mu \hat{\mu})} = \int \frac{d^4p}{(2\pi)^4} \tilde{\phi}(p) e^{i(p_\mu x_\mu + aN p_\mu \hat{\mu} + 2\pi l_\mu \hat{\mu})}, \quad l_\mu \in \mathbb{Z}^4
\end{aligned}
\tag{3.7}
$$

which implies that

$$e^{i(ap_\mu \hat{\mu}N + 2\pi l_\mu \hat{\mu})} = 1, \tag{3.8}$$

leading to the discretization of the momenta:

$$p_\mu = \frac{2\pi l_\mu}{aN}. \tag{3.9}$$

Moreover, since

$$e^{ip_\mu x_\mu} = e^{i(p_\mu x_\mu + 2\pi n_\mu \hat{\mu})} = e^{i(p_\mu + \frac{2\pi}{a}\hat{\mu})x_\mu}, \tag{3.10}$$

the Fourier transform (3.5) is periodic in momentum space and can be restricted to $-\frac{\pi}{a}\hat{\mu} < p_\mu \leq \frac{\pi}{a}\hat{\mu}$. It then follows that

$$p_\mu = \frac{2\pi l_\mu}{aN}, \quad l_\mu \in \left\{(-N/2)+1, ..., N/2\right\}_\mu. \tag{3.11}$$

Therefore, not only is the momenta discretized, but also bounded. This serves as the high energy cut-off, and since the lattice volume V serves as a high distance (low energy) cut-off, a lattice theory is naturally regularized, such that when the lattice spacing a is given units, the scale ambiguity is dealt with, as was mentioned at the end of section 1.1.

The continuous integral over the momenta in Fourier transform (3.5) can now be converted to the discrete finite sum

$$\phi(x) = \frac{1}{V} \sum_{l_\mu} e^{ip_\mu \cdot x_\mu} \tilde{\phi}(p). \tag{3.12}$$

Furthermore, the measure $\mathcal{D}[\phi]$ in (3.2) becomes a finite product over the lattice volume,

$$\mathcal{D}[\phi] = \prod_x^V d\phi_\alpha(x), \tag{3.13}$$

such that the configuration space integration is now of finite dimension and, in principle, one can perform numerical integration. Due to the high dimension of this integration, a practical approach is the statistical method of Monte Carlo integration.

We, therefore, see how the lattice formulation leads to the practical possibility of computing the correlation function. Still, one needs to formulate the gauge invariant quantum field theory on the lattice, i.e. find the lattice action such that in the continuum limit, it corresponds to the continuum theory, which in this case will be QCD.

3.3   Quenched Quantum Chromodynamics Lattice Action

To formulate QCD on the lattice, we use colour gauge symmetry as a guiding principle (see Section 1.2) to find an action that, in the continuum limit, corresponds to its physical continuum space-time version. In what follows, we will not take into account the quarks dynamics and consider only the pure gauge sector of QCD, known as quenched QCD, which is motivated by the alleviation of computer resources and reasonable estimates for quenching errors [2].

Start with defining the lattice version of the link variable (1.22) as

$$U_\mu(x) = \mathcal{P}\left\{ \exp\left(ig \int_x^{x+a\hat{\mu}} dl^\nu A_\nu(x+dl) \right) \right\}, \tag{3.14}$$

the link variable $U_\mu(x)$ is now a field orientated towards μ and connecting the lattice points between x and $x+a\hat{\mu}$. By considering a small lattice spacing[9], such that the distance between x and $x+a\hat{\mu}$ is small, one can approximate this path-integral by

$$U_\mu(x) = e^{iagA_\mu(x+\frac{\hat{\mu}}{2})}, \tag{3.15}$$

following the adjoint representation transformation

$$U_\mu(x) \longrightarrow V(x)U_\mu(x)V(x+\hat{\mu}), \tag{3.16}$$

with

$$V_{ij}(x) \equiv \exp[i\theta^a(x)t^a], \tag{3.17}$$

---

[9]Note that the notion of a "small" lattice spacing only makes sense in the continuum extrapolation, i.e. $a \longrightarrow 0$.
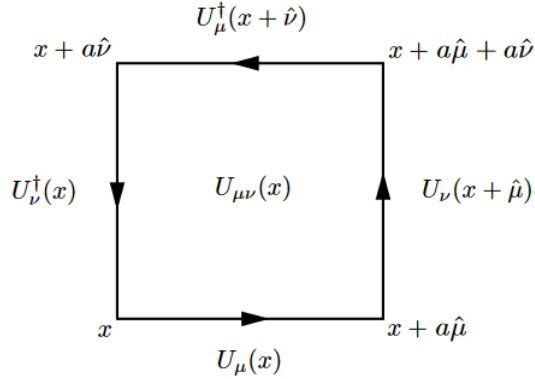
Figure 3.1: Graphical representation of the construction of the *plaquette* $U_{\mu\nu}(x)$, on the $\mu - \nu$ plane, by multiplying links in a closed loop.

where $A_\mu = t^a A^a_\mu$, just as was done in the continuum case. Although fermions will be neglected in this work, the link variable serves the same purpose as in the continuum case, where one needs to be able to compare field values at different sites in a gauge-invariant way.

The link field (3.15) enables one to build the colour gauge symmetric action whose continuum limit is the Euclidean Yang-Mills action (see 1.34),

$$S_{\text{YM}}[F] = \int d^4x \, \frac{1}{2} Tr(F_{\mu\nu} F_{\mu\nu}).$$

(3.18)

The simplest one is the Wilson action [63], and it is built from

$$U_{\mu\nu}(x) = U_\mu(x) U_\nu(x + \hat{\mu}) U_\mu^\dagger(x + \hat{\nu}) U_\nu^\dagger(x),$$

(3.19)

known as a *plaquette*, pictorially represented in Figure 2.1. By using the link's gauge transformation (3.16) in the *plaquette*, one sees that

$$U_{\mu\nu}(x) \longrightarrow V(x) U_{\mu\nu}(x) V^\dagger(x),$$

(3.20)

such that we can build the gauge symmetric colour trace,

$$Tr\left[U_{\mu\nu}(x)\right] \longrightarrow Tr\left[V(x) U_{\mu\nu}(x) V(x)\right] = Tr\left[U_{\mu\nu}(x)\right].$$

(3.21)

The Wilson action can now be built by applying the Baker-Campbell-Hausdorff formula,

$$e^A e^B = e^{A + B + \frac{1}{2}[A,B] + \cdots}$$

(3.22)

in the *plaquette* (3.19), and Taylor expanding, that leads to

$$U_{\mu\nu}(x) = \exp\{ia^2 g F_{\mu\nu}(x) + \mathcal{O}(a^3)\},$$

(3.23)

17

where we find the lattice version of the field-strength tensor,

$$F_{\mu\nu}(x) \equiv \partial_\mu A_\nu - \partial_\nu A_\mu - ig[A_\mu, A_\nu], \tag{3.24}$$

with ∂_μ being the lattice derivative,

$$\partial_\mu A_\nu(x) = \frac{A_\nu(x + \hat{\mu}) - A_\nu(x)}{a}. \tag{3.25}$$

The new *plaquette* expression's exponential (3.23) can now be expanded in powers of a,

$$U_{\mu\nu}(x) = I + ia^2 g F_{\mu\nu} - \frac{a^4}{2} g^2 F_{\mu\nu}^2 + \mathcal{O}(a^5), \tag{3.26}$$

and seeing as one is trying to reach the discretization of the continuum Yang-Mills action (3.18), from the previous expression, the Wilson action can be written as the sum over all the lattice's *plaquettes* of one orientation,

$$\begin{aligned}
S_W[U] &= \beta \sum_x \sum_{\mu < \nu} \operatorname{Re} Tr \left(I - U_{\mu\nu}(x) \right) \\
&= \sum_x \sum_{\mu < \nu} \frac{a^4}{2} Tr \left(F_{\mu\nu}^2 \right) + \mathcal{O}(a^5),
\end{aligned} \tag{3.27}$$

where $\beta = 1/g^2$ and in the last equality, the discretized version of S_{YM} is identified, with the integral replaced by the lattice sum with a factor of a^4. Thus, the continuum limit of the Wilson action is the Yang-Mills action. However, there is no reason why the continuum limit requirement of Wilson's, or any other action, should ensure that this theory corresponds to QCD. As such, the continuum extrapolation of the lattice theory, $a \longrightarrow 0 \, V \longrightarrow \infty$, needs further investigation [55, 57].

3.3.1 The Continuum Limit and Scale

The Wilson action (3.27) shows that the bare coupling constant g is the free parameter. It serves as the available fine-tuning for extrapolating the lattice theory to the continuum by removing the regulator, i.e. when the lattice spacing is set to zero. Physical predictions are independent of this procedure, i.e. for a given dimensionful lattice computed observable $\Theta(a, g(a))$,

$$\lim_{a \longrightarrow 0} \Theta(a, g(a)) = \Theta_{\mathrm{phys}}, \tag{3.28}$$

with Θ_{phys} the physical quantity. This gives rise to the renormalization group formalism [61], where one finds the solution $g(a)$ from the differential equation

$$\frac{d \, \Theta(a, g(a))}{d \ln a} = 0, \tag{3.29}$$

whose integration constant Λ sets the lattice spacing scale by fixing the value of g for a given a to achieve the continuum extrapolation.

This work's lattice calculations reported in Chapter 4 were performed using the Wilson action (3.27), where the scale is set from the physical data taken from lattice simulation results on the static quark-antiquark potential [6], corresponding to $\beta = 6.0$ and $a = 0.1016(25)$ fm, equivalent to $1/a = 1.943(48)$ GeV. The uncertainty on the lattice spacing will be discarded in the results of this work.

3.3.2 Gauge Fixing

Section 1.2.1 showed the necessity to gauge fix to have a well-defined theory and compute the Green functions due to the $A_\mu(x)$ integration over the gauge orbit (1.36). In the lattice formulation, $U_\mu(x)$ is now the integration variable in the computation of correlation functions,

$$\langle \mathcal{O} \rangle = \frac{\int \mathcal{D}[U]\,\mathcal{O}(U)\,e^{-S_W[U]}}{\int \mathcal{D}[U]e^{-S_W[U]}}. \tag{3.30}$$

Even though physical predictions are gauge-independent, correlation functions are gauge-dependent. Therefore, studying these quantities requires specifying a gauge. In Chapter 2, it was seen how the four gluon vertex is extracted from the four gluon correlation function in the Landau gauge, and seeing as this work intends to investigate this vertex on the lattice, this requires computing the correlation functions in this gauge.

The continuum Landau gauge fixing condition, $\partial_\mu A_\mu(x) = 0$, is realized on the lattice if $U_\mu(x)$ is a stationary point, with respect to gauge transformations $V(x)$, of the functional

$$F_U[V] = \frac{1}{12V} \sum_{\mu,x} \operatorname{Re} Tr\left(V(x)U_\mu(x)V^\dagger(x+\hat\mu)\right), \tag{3.31}$$

which can be seen by writing $V(x)$ as an infinitesimal transformation in the previous expression and using the link variable definition (3.14). This gauge condition has multiple solutions [27], i.e. in a given gauge orbit, the gauge field transformation satisfying the previous expression is not unique. As was mentioned in Section 1.3, these are known as Gribov copies, and in [40], it is shown that their presence leads to ill-defined lattice expectation values of gauge-fixed correlation functions due to the integration over the configuration space being zero. This is known as the Neuberger 0/0 problem.

To overcome this, one can define the lattice region of Landau gauge-fixed configurations

$$\Gamma \equiv \{U_\mu : \partial_\mu A_\mu = 0\}, \tag{3.32}$$

and the Fundamental Modular Region $\Lambda \subset \Gamma$ [64], defined by the set of link variables corresponding to absolute maxima of the functional (3.31). In [14, 52] it is seen that the effect of Gribov copies in this region is small.

3.4 Correlation Functions from Monte Carlo simulations

In Chapter 2, it was seen that one could span the gluon correlation functions on a tensor basis and how the form factors defined the correlation function on the basis (2.1). Lattice computations evaluate scalar observables (3.30) and, as such, evaluating a gluon correlation function on the lattice is equivalent to computing its form factors. In Chapter 2, it was also seen how these form factors could be found from Lorentz-colour contractions of correlation functions with their respective tensor basis elements, in particular, for the gluon propagator (2.6) and the four gluon correlation function (2.22)[10]. These form factors are the lattice observables to be computed.

---

[10]Note that these expressions were defined in the continuum. On the lattice, the $(2\pi)^4$ factor is replaced by the lattice volume V and $\delta(0) = 1$.

The Euclidean space-time path integral allows the usage of statistical methods to perform such computations. Having developed the Wilson action, the required functional integration in the computation of lattice observables (3.30) can now be approximated with Monte Carlo integration,

$$\langle \mathcal{O} \rangle = \frac{\int \mathcal{D}[U]\, \mathcal{O}[U]\, e^{-S_W[U]}}{\int \mathcal{D}[U] e^{-S_W[U]}} \approx \frac{1}{N} \sum_{i=1}^{N} \mathcal{O}(U_i), \tag{3.33}$$

since the law of large numbers ensures that

$$\lim_{N \longrightarrow \infty} \langle \mathcal{O} \rangle = \frac{1}{N} \sum_{i=1}^{N} \mathcal{O}(U_i). \tag{3.34}$$

Here, $\{U_i\}$ is the ensemble of link variables configurations[11] generated by the creation of a Markov Chain whose equilibrium distribution is

$$P(U) = \frac{e^{-S_W[U]}}{\int \mathcal{D}[U] e^{-S_W[U]}}. \tag{3.35}$$

This enables the computation of the gluon correlation function's form factors. To do so, one needs to be able to relate the link variables to the gluon fields. This can be done by expanding the link variable defined in (3.15),

$$A_\mu(x + \hat{\mu}/2) = \frac{1}{2ig}[U_\mu(n) - U_\mu^\dagger(n)] - \frac{1}{6ig} Tr[U_\mu(n) - U_\mu^\dagger(n)] + \mathcal{O}(a^2), \tag{3.36}$$

where the trace term was added such that $Tr(A_\mu) = 0$ and the lattice spacing has been absorbed into A_μ. Fourier transforming the gauge fields to momenta space,

$$A_\mu(p) = V \sum_x e^{-ip \cdot (x + \hat{\mu}/2)} A_\mu(x + \hat{\mu}/2). \tag{3.37}$$

Having generated the previous momentum-space gauge fields for each configuration, the form factors of the gluon propagator (2.6) and four gluon correlation function (2.22) can now be computed.

The computer code used to implement the Landau gauge fixing procedure and generate gauge fields uses both Chroma [21] and PFFT [46] libraries. Details on these computation methods can be found in [18, 19, 43].

3.5   Error Analysis and Correction Methods

Lattice simulation results are affected by different sources of errors, both systematic and statistical. These must be dealt with.

As seen previously, the computation of observables is carried out using sampling techniques. The

---

[11]A link variable configuration is defined by the set of all the values of $U_\mu(x)$ on a given lattice, i.e. the assignments of $SU(3)$ matrices to all the lattice points.

algorithmic performance and the available computer power limit these. This introduces statistical errors due to the finite number of configurations since the law of large (3.34) numbers cannot be verified. Therefore, one is limited by the data required for analysis and forced to improve the signal-to-noise ratio of the obtained results.

Systematic errors, however, are much more subtle and require a significant investment from lattice studies to control and reduce them. These become noticeable when computation resources allow for negligible statistical errors. The systematic errors manifest themselves according to the chosen lattice action and the continuum extrapolation approach. From the previous sections, the sources of such errors can be understood to be due to the effects of finite volume, lattice spacing, and the quenched approximation. This dissertation will consider only errors due to finite lattice spacing, known as lattice artefacts, and statistical errors.

3.5.1 Lattice Artefacts

Lattice artefacts are expressed in numerous ways. In this work, the lattice-extracted data will be the aforementioned named form factors. These Euclidean continuum space-time scalar functions can only depend on the momentum variable p^2, such that they are invariant under the orthogonal transformations of the $O(4)$ group, which preserves the scalar product and, therefore, have p^2 as one of its invariants. When space-time is discretized, the continuous rotational symmetry is broken, imposing fewer space-time symmetry constraints on the momenta dependence of the lattice-evaluated form factors. This is the lattice artefact manifestation that will be considered in this work. Note that there is a discussion to be had on the effect of this symmetry breaking in the correlation functions tensor basis description [58]. In Chapter 2, the four gluon correlation function tensor description was formulated in the continuum. On the lattice, such a prescription is lacking. This issue will not be considered here due to the high complexity of the four-gluon correlation function tensor structure.

On the hypercubic lattice, this symmetry breaking reduces the $O(4)$ group to the hypercubic subgroup $H(4)$, comprised of $\pi/2$ rotations and parity transformations. Whilst the former group transformations preserved p^2, the latter preserves[12] [1]

$$p^{[2n]} = \sum_\mu p_\mu^{2n}, \quad n \in \{1, 2, 3, 4\}. \tag{3.38}$$

Therefore, the lattice form factors will not solely be functions of the $O(4)$ invariant p^2, as in the continuum case, but now gain the additional freedom to depend on the $H(4)$ group invariants,

$$F(p^2) \xrightarrow[lattice]{} F(p^2, p^{[4]}, p^{[6]}, p^{[8]}). \tag{3.39}$$

Ergo, after computing the lattice form factors $F(p^2)$ for every possible of p_μ on the lattice (3.11), the form factor values corresponding to equal values of p^2 will not necessarily be equal due to their new dependence on the $H(4)$ invariants degrees of freedom

$$F(p^2) \neq F(p^2, p^{[4]}, p^{[6]}, p^{[8]}). \tag{3.40}$$

---

[12]In d-dimensions, $n \in \{1, 2, ..., d\}$.

The previously described effects, associated with the breaking of rotational symmetry, can be handled if the lattice momenta $p_\mu = (p_1, p_2, p_3, p_4)$ are restricted to

$$p_\mu \in \big\{ (\pm p_1, 0, 0, 0),\, (\pm p_1, \pm p_1, 0, 0),\, (\pm p_1, \pm p_1, \pm p_1, 0),\, (\pm p_1, \pm p_1, \pm p_1, \pm p_1) \big\}. \tag{3.41}$$

It follows that, for two different momenta p'_μ and p''_μ belonging to the previous set,

$$p'^2 = p''^2 \implies p'^{[4]} = p''^{[4]}, \quad p'^{[6]} = p''^{[6]}, \quad p'^{[8]} = p''^{[8]}, \tag{3.42}$$

and the new degrees of freedom that rose out of the continuous rotational symmetry breaking become redundant and can be removed,

$$F(p^2, p^{[4]}, p^{[6]}, p^{[8]}) = F(p^2). \tag{3.43}$$

A signal-to-noise improvement can be made by considering the degeneracy of the lattice form factors with the same $H(4)$ invariants, or the same p^2 with the momentum-space cut (3.41), and averaging them.

3.5.2 Bootstrap Method

Due to the finite amount of data and lack of information on the error propagation in the sampling methods, there is the need for a reliable method for statistical error estimation that deals with these issues. The bootstrap method, which is a distribution-independent technique that assumes uncorrelated data, was chosen for statistical error estimation. A comprehensive view of this method can be found in [22].

Bootstraping starts by performing $K = N_b \times N$ random samplings with replacement of the original ensemble $\{\mathcal{O}(U_i)\}$, where $i = 1, 2, ..., N$ and N_b is a chosen number. These bootstrap samples generate a new ensemble $\{\mathcal{O}_j(U_k)\}$, where $j = 1, 2, ..., K$ and k is random number between 1 and N that is allowed to be repeated. This new ensemble now provides an estimation of the original $\{\mathcal{O}(U_i)\}$ ensemble distribution and one can define average

$$\langle \mathcal{O} \rangle_B = \sum_{j=1}^{K} \frac{\mathcal{O}_j(U_k)}{K}. \tag{3.44}$$

The error can now be estimated by defining the uncertainty bounds

$$\sigma_u = \mathcal{O}_u - \langle \mathcal{O} \rangle_B, \quad \sigma_d = \langle \mathcal{O} \rangle_B - \mathcal{O}_d, \quad \mathcal{O}_d, \mathcal{O}_u \in \{\mathcal{O}_j(U_k)\}, \tag{3.45}$$

with $\mathcal{O}_d$ and $\mathcal{O}_u$ satisfying

$$\frac{\#\{x < \mathcal{O}_u : \forall x \in \{\mathcal{O}_j(U_k)\}\}}{K} = \frac{C+1}{2}, \quad \frac{\#\{x < \mathcal{O}_d : \forall x \in \{\mathcal{O}_j(U_k)\}\}}{K} = \frac{C-1}{2}. \tag{3.46}$$

Here, $\#\{...\}$ stands for the cardinality of the set and $C \in [0, 1]$ expresses the confidence interval, this work will set $C = 0.65$. It follows that the lattice computed data can now be given an uncertainty,

$$\langle \mathcal{O} \rangle \pm \max\{|\sigma_u|, |\sigma_d|\}. \tag{3.47}$$

4. Form Factors Data and Results

This chapter reports and discusses this work's lattice-computed four gluon correlation function and vertex bare form factors, investigated in the specific kinematic configurations (2.24),

$$(p, p, p, -3p), \quad (0, p, p, -2p), \quad (0, p, 2p, -3p). \tag{4.1}$$

All the following data statistical errors were estimated with the bootstrap method. The reader is again reminded that the following form factors do not originate from a complete basis tensor basis, except for $(p, p, p, -3p)$, and as such, there is a possibility for unknown contributions to this data.

4.1 Lattice Setup

To summarize this work's lattice simulation setup, the lattice Landau gauge (3.31) constrained link variable configurations $\{U_i\}$ were generated by Monte Carlo sampling using the Wilson Action (3.27), with $\beta = 6.0$ and $a = 0.1016$ fm. These configurations were also used in [18, 19, 43].

This work computed form factors with 2000 configurations in a lattice volume of 64^4 points, 1801 configurations in a volume of 80^4 and 4620 configurations in a volume of 32^4. Only in the latter volume was the signal-to-noise ratio acceptable and the data suitable to be discussed, and as such, the following results are established in this volume, i.e. every form factor was found by performing an ensemble average over 4620 configurations and in a lattice volume of 32^4 lattice points.

4.2 Four Gluon Correlation Function Form Factors

This section reports on what is this work's lattice-accessible data – the four gluon correlation function form factors. These were computed with the ensemble average expressions found at the end of Appendix B. Herein, all data is the result of an average over the form factors with equal $H(4)$ invariants and, due to the small amount of data in the infrared region, only for $p > 0.7 GeV$ are the momenta cuts in (3.41) applied. Ergo, this chapter will not contain the full lattice-extracted data, i.e. the correlation function form factors. Appendix C provides the full lattice ensemble-averaged four gluon correlation function form factor data, free from momentum-space cuts and averages over the $H(4)$ invariants degeneracy. Moreover, Appendix C shows the lack of signal-to-noise ratio that was improved with the momentum-space cuts.

Due to the large difference in the order of magnitude of the form factors values, a zoomed-in

version of the full data plots will be used, with the axes of plots next to one another representing the same quantities and units; therefore, the zoomed-in plot axes labels are omitted. This will be the convention throughout this work's plotted data.
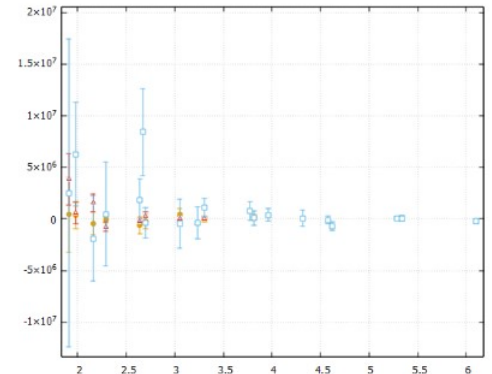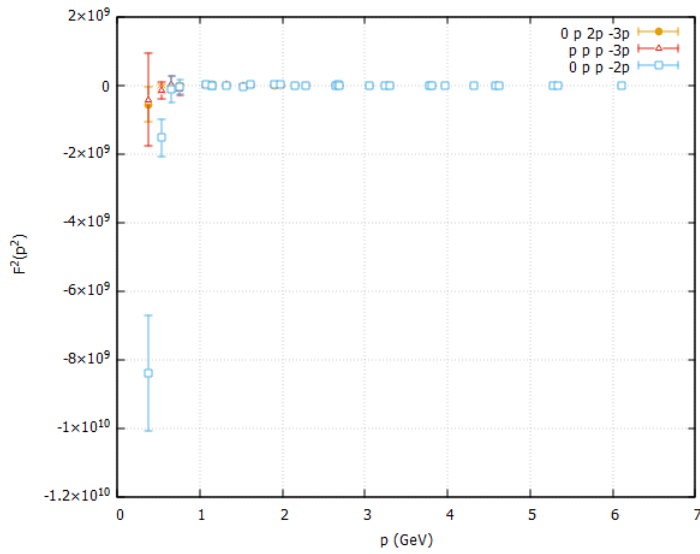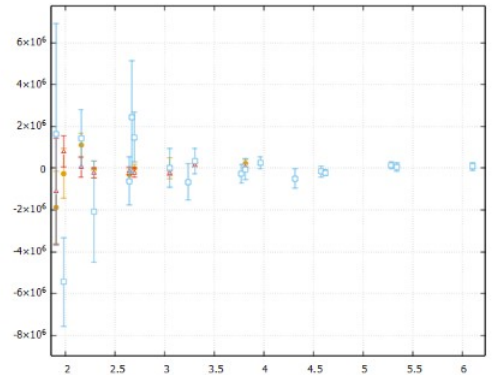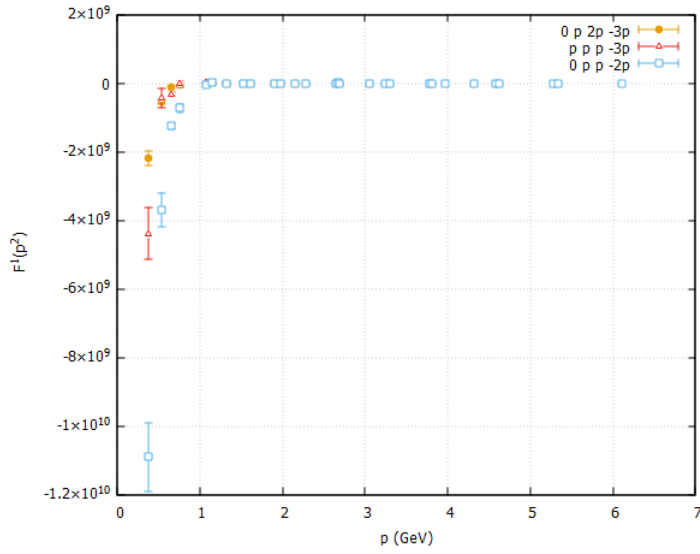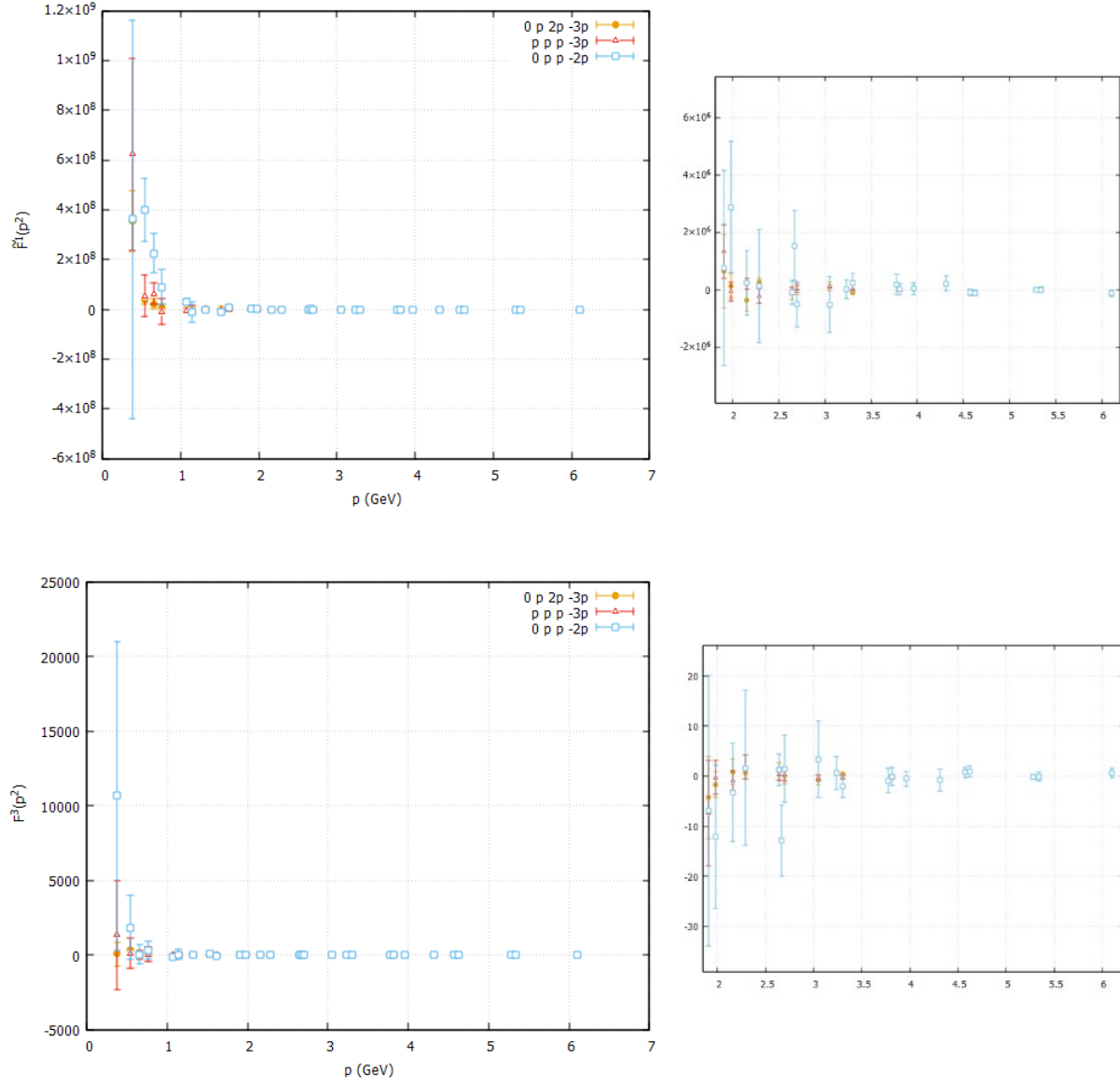
Figure 4.1: The real part of the computed four gluon correlation function bare form factors $F^{(1)}(p^2)$, $F^{(2)}(p^2)$, $\tilde{F}^{(1)}(p^2)$ and $F^{(3)}(p^2)$, on a lattice of volume 32^4. The plot on the left contains all the computed data, whilst the plot on the right is a zoom-in version of the left plot.

When the average over the form factor with the same $H(4)$ invariants is performed, the imaginary part of the form factors vanishes; therefore, the plotted data only shows their real part.

25

The form factor $F^{(3)}$, of the basis tensor $t^{(3)}$, is found from the linear combination (2.17) to be

$$F^{(3)}(p^2) = c_1 \widetilde{F}^{(1)} - c_2 F^{(1)} - c_3 F^{(2)}, \tag{4.2}$$

where c_1, c_2 and c_3 are real numbers found from tensor contractions, see Appendix B. Due to $F^{(1)}$, $F^{(2)}$ and $\widetilde{F}^{(1)}$ being of the same order of magnitude, and equally for c_1, c_2 and c_3, the previous expression explains the heavy suppression of $F^{(3)}$ in figure 4.1, in comparison to $F^{(1)}$ and $F^{(2)}$.

The plotted data shows significant statistical errors, and by comparing data points of equal order of magnitude, one sees that the error bars are, in general, particularly big for the $(p, p, p - 3p)$ configuration. This can be understood by inspection of the expressions in Appendix B, where the ensemble average for this kinematic configuration requires fewer terms than the others, giving rise to more significant statistical fluctuations, since by including a higher number of terms in the ensemble averaging, the statistical fluctuations are expected to be averaged out. This statistical error can be diminished by increasing the number of configurations in the ensemble.

The data shows an acceptable signal for $p < 1$ GeV, which is lost for higher momenta values. $F^{(1)}(p^2)$ showed the better signal in this momenta range. The overall form factors signal can be improved by considering a larger lattice volume, whereby increasing the number of lattice points, the available data in the previously plotted momenta range would also increase.

4.3 Four Gluon Vertex Form Factors

This section presents and discusses the data of main importance to this dissertation – the four gluon vertex function form factors. In section 2.3.2, it was seen that these are found by dividing the previous four gluon correlation form factors by the gluon propagator form factors associated with the external legs,

$$\bar{F}^{(i)}(p^2) = \frac{F^{(i)}}{g^{\mu'\mu}g^{\nu'\nu}g^{\eta'\eta}g^{\zeta'\zeta}D_{\mu\mu'}^{aa'}(p_1)D_{\nu\nu'}^{bb'}(p_2)D_{\eta\eta'}^{cc'}(p_3)D_{\zeta\zeta'}^{dd'}(p_4)t_{\mu'\nu'\eta'\zeta'}^{(i)abcd}t_{a'b'c'd'}^{(i)\mu'\nu'\eta'\zeta'}}. \tag{4.3}$$

The tensor contractions in the denominator are computed in Appendix B. Appendix C presents the gluon propagator form factors, also computed in the 32^4 lattice volume and with the 4620 ensemble average. The propagator form factor statistical errors are minute compared to the four gluon correlation function form factors errors and were therefore ignored in this work.
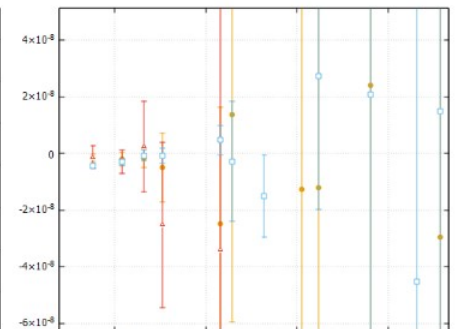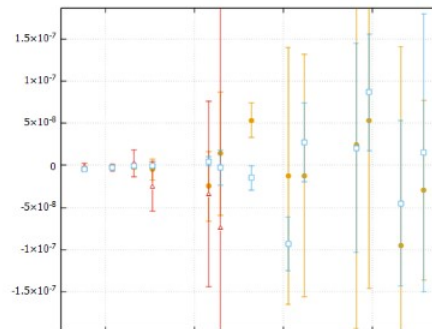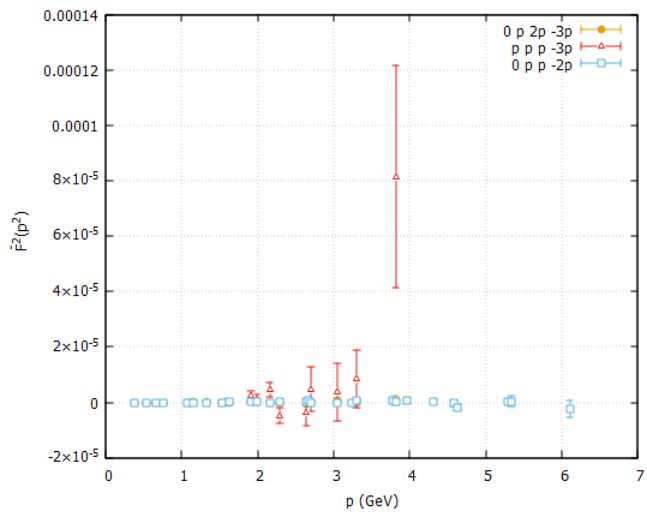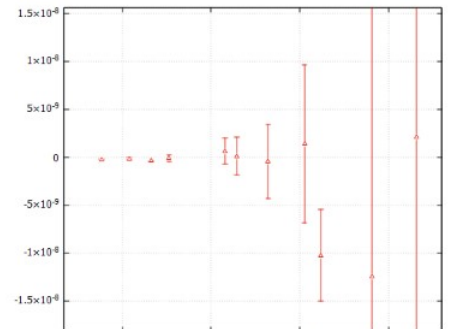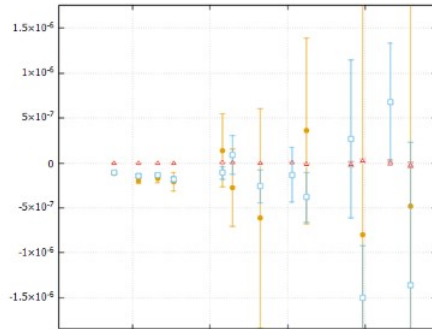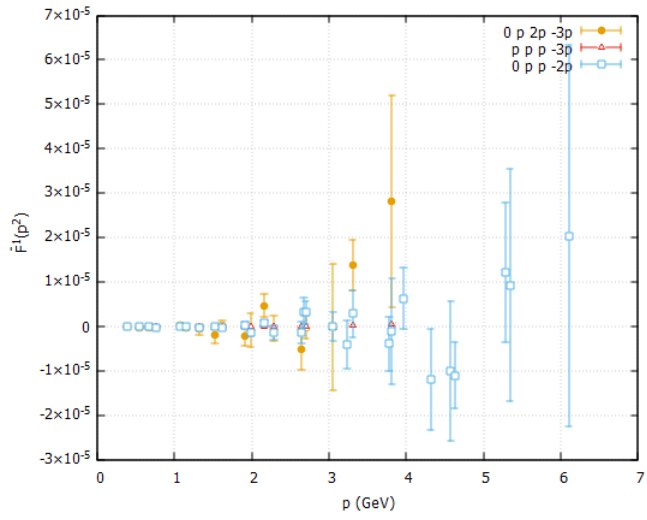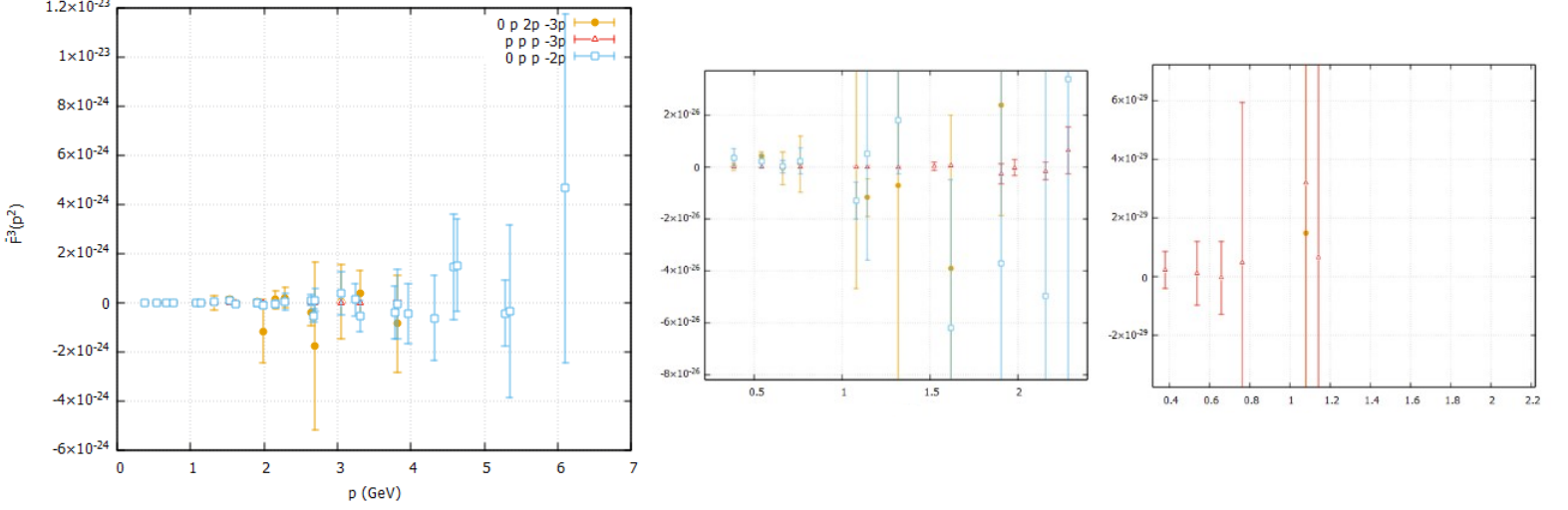
Figure 4.2: The real part of the computed four gluon vertex function bare form factors $\bar{F}^{(1)}(p^2)$, $\bar{F}^{(2)}(p^2)$ and $\bar{F}^{(3)}(p^2)$, on a lattice of volume 32^4. The plot on the far left contains all the computed data, whilst the two plots on the right are a zoom-in version of the far left plot.

In the last section, it was seen that the four gluon correlation function form factors decreased with increasing momenta scale, but here, the vertex form factors increased with the momenta. This can be understood due to the propagator form factors in (2.23) and their behaviour in the momenta scale, see Appendix C.

Although this data should be read carefully due to the weak signal and high statistical errors, it is clear that the vertex form factor $\bar{F}^{(3)}$ is heavily suppressed in this momenta range and in all kinematic configurations. This suppression is even more evident in the configuration of particular interest, $(p, p, p, -3p)$. $\bar{F}^{(1)}$ data shows that it is heavily suppressed in the kinematic $(p, p, p, -3p)$, and only contributions in the $(0, p, p, -2p)$ and $(0, p, 2p, -3p)$ configurations. In these kinematics, the form factors appear to rise with the momenta, although only in the $(0, p, p, -2p)$ is the signal-to-noise ratio good enough to draw decisive conclusions.

Relative to $\bar{F}^{(1)}$, the form factor $\bar{F}^{(2)}$ displays a contrast difference in its dependence on the chosen kinematic configuration. Here, the data shows that $\bar{F}^{(2)}$ is suppressed in $(0, p, p, -2p)$ and $(0, p, 2p, -3p)$, with the only contribution coming in $(p, p, p, -3p)$, where the the acceptable signal-to-noise ration shows that it rises with increasing momenta. The difference between the behaviour of $\bar{F}^{(1)}$ and $\bar{F}^{(2)}$ in the kinematic $(p, p, p, -3p)$ is of utmost interest, seeing as in this kinematic configuration, the tensor basis is complete.

To end this chapter, notice that the lattice gauge fields A_μ contain a factor of the lattice spacing a (3.36). It follows that a can be factored out of the ensemble average in the lattice four gluon vertex

computations,

$$\frac{a^4 \langle A\,A\,A\,A \rangle}{\left(a^2 \langle A\,A \rangle\right)^4} = \frac{\langle A\,A\,A\,A \rangle}{a^4 \left(\langle A\,A \rangle\right)^4} \tag{4.4}$$

To make a connection to non-lattice studies, this factor can be cancelled by the redefinition

$$\frac{a^4 \langle A\,A\,A\,A \rangle}{\left(a^2 \langle A\,A \rangle\right)^4} \longrightarrow a^4\,\frac{a^4 \langle A\,A\,A\,A \rangle}{\left(a^2 \langle A\,A \rangle\right)^4}, \tag{4.5}$$

i.e. a constant global factor in the form factor data.

5. Summary and Conclusions

Non-perturbative information on the behaviour of the four gluon vertex is severely lacking. This dissertation aimed to investigate the four gluon vertex from Lattice QCD. This formalism can only access the four correlation function form factors. Hence, Chapter 2 was dedicated to formulating the needed expressions and conditions to allow us to do these computations. After establishing the required lattice formalism in Chapter 3, the following chapter showed and discussed our results.

This was exploratory research and proof that one could study the four gluon vertex from lattice QCD. The data reported is novel, and as such, considerations must be taken lightly, not only due to the small number of other works to compare the data but also because statistical errors and signal-to-noise ratio problems hinder the results. Nevertheless, the data showed the effectiveness of our lattice simulations and results of satisfactory quality, from which conclusions can be drawn. This data shows that two of the form factors $\bar{F}^{(1)}$ and $\bar{F}^{(2)}$) contribute vastly more than $\bar{F}^{(3)}$ to the vertex. The interplay between the form factor values and the chosen kinematic configuration can also be analyzed. Moreover, the external legs gluon propagators' contribution is evident when comparing the four gluon correlation function and vertex form factors. Special emphasis is put on the considered tensor basis being only complete for the kinematic $(p, p, p, -3p)$.

Not only can our data gathered on the four gluon vertex be improved by upgrading the lattice setup, i.e. by using more ensemble configurations and a larger lattice volume, but other studies can build on or supplement the data found in this work. Self-imposed limitations were set in the form of kinematic configurations and basis tensor structures that allowed the practical implementation of lattice simulations, and future coverage over a more complete set of kinematics and tensors may be possible. Nevertheless, lattice data on this vertex is first needed before delving into more intricate and realistic degrees of freedom.

Bibliography

[1] *The Classical Groups: Their Invariants and Representations*. Princeton University Press, 1966.

[2] Light hadron spectrum and quark masses from quenched lattice QCD. *Phys. Rev. D*, 67:034503, Feb 2003.

[3] A. C. Aguilar, F. De Soto, M. N. Ferreira, J. Papavassiliou, J. Rodríguez-Quintero, and S. Zafeiropoulos. Gluon propagator and three-gluon vertex with dynamical quarks. *The European Physical Journal C*, 80(2), feb 2020.

[4] A. C. Aguilar, D. Binosi, D. Ibañez, and J. Papavassiliou. New method for determining the quark-gluon vertex. *Physical Review D*, 90(6), sep 2014.

[5] R Alkofer and J Greensite. Quark confinement: the hard problem of hadron physics. *Journal of Physics G: Nuclear and Particle Physics*, 34(7):S3–S21, may 2007.

[6] Gunnar S. Bali and Klaus Schilling. Running coupling and the Λ parameter from SU(3) lattice simulations. *Phys. Rev. D*, 47:661–672, Jan 1993.

[7] James S. Ball and Ting-Wai Chiu. Analytic properties of the vertex function in gauge theories. II. *Phys. Rev. D*, 22:2550–2557, Nov 1980.

[8] Jürgen Berges. n-particle irreducible effective action techniques for gauge theories. *Phys. Rev. D*, 70:105010, Nov 2004.

[9] D. Binosi, D. Ibañez, and J. Papavassiliou. Nonperturbative study of the four gluon vertex. *Journal of High Energy Physics*, 2014(9), sep 2014.

[10] Adrian L. Blum, Reinhard Alkofer, Markus Q. Huber, and Andreas Windisch. Three-point vertex functions in Yang-Mills Theory and QCD in Landau gauge. *EPJ Web of Conferences*, 137:03001, 2017.

[11] N. Brambilla et al. QCD and Strongly Coupled Gauge Theories: Challenges and Perspectives. *Eur. Phys. J. C*, 74(10):2981, 2014.

[12] Guilherme Telo R. Catumba. Gluon correlation functions from lattice quantum chromodynamics, 2021.

[13] Attilio Cucchieri, Axel Maas, and Tereza Mendes. Three-point vertices in Landau-gauge Yang-Mills theory. *Physical Review D*, 77(9), may 2008.

[14] Attilio Cucchieri and Tereza Mendes. 1) The influence of Gribov copies on gluon and ghost propagators in Landau gauge and 2) A new implementation of the fourier acceleration method. *Nuclear Physics B - Proceedings Supplements*, 63(1-3):841–843, apr 1998.

[15] Anton K. Cyrol, Leonard Fister, Mario Mitter, Jan M. Pawlowski, and Nils Strodthoff. Landau gauge Yang-Mills correlation functions. *Phys. Rev. D*, 94(5):054005, 2016.

[16] Anton K. Cyrol, Markus Q. Huber, and Lorenz von Smekal. A Dyson–Schwinger study of the four-gluon vertex. *The European Physical Journal C*, 75(3), mar 2015.

[17] G. Dissertori, I. G. Knowles, and M. Schmelling. *High energy experiments and theory.* 2003.

[18] Anthony G. Duarte, Orlando Oliveira, and Paulo J. Silva. Lattice gluon and ghost propagators and the strong coupling in pure SU(3) Yang-Mills theory: Finite lattice spacing and volume effects. *Physical Review D*, 94(1), jul 2016.

[19] David Dudal, Orlando Oliveira, and Paulo J. Silva. High precision statistical Landau gauge lattice gluon propagator computation vs. the Gribov–Zwanziger approach. *Annals of Physics*, 397:351–364, oct 2018.

[20] N. Dupuis, L. Canet, A. Eichhorn, W. Metzner, J.M. Pawlowski, M. Tissier, and N. Wschebor. The nonperturbative functional renormalization group and its applications. *Physics Reports*, 910:1–114, may 2021.

[21] Robert G. Edwards and Balint Joo. The Chroma software system for lattice QCD. *Nucl. Phys. B Proc. Suppl.*, 140:832, 2005.

[22] Bradley Efron and Robert J. Tibshirani. *An Introduction to the Bootstrap*. Number 57 in Monographs on Statistics and Applied Probability. Chapman & Hall/CRC, Boca Raton, Florida, USA, 1993.

[23] Gernot Eichmann, Christian S. Fischer, and Walter Heupel. Four-point functions and the permutation group S4. *Physical Review D*, 92(5), sep 2015.

[24] Gernot Eichmann, Richard Williams, Reinhard Alkofer, and Milan Vujinovic. Three-gluon vertex in Landau gauge. *Physical Review D*, 89(10), may 2014.

[25] William Fulton. *Young Tableaux: With Applications to Representation Theory and Geometry.* London Mathematical Society Student Texts. Cambridge University Press, 1996.

[26] Christof Gattringer and Christian B. Lang. *Quantum chromodynamics on the lattice*, volume 788. Springer, Berlin, 2010.

[27] L. GIUSTI, M. L. PACIELLO, S. PETRARCA, B. TAGLIENTI, and C. PARRINELLO. PROBLEMS ON LATTICE GAUGE FIXING . *International Journal of Modern Physics A*, 16(21):3487–3534, aug 2001.

[28] Yann Gouttenoire. Beyond the Standard Model Cocktail, 2022.

[29] J. A. Gracey. Symmetric point quartic gluon vertex and momentum subtraction. *Physical Review D*, 90(2), jul 2014.

[30] V. N. Gribov. Quantization of Nonabelian Gauge Theories. *Nucl. Phys. B*, 139:1, 1978.

[31] Howard Haber. Useful relations among the generators in the defining and adjoint representations of SU(N). *SciPost Physics Lecture Notes*, jan 2021.

[32] Markus Q. Huber. Nonperturbative properties of Yang-Mills theories, 2020.

[33] Markus Q. Huber. Correlation functions of Landau gauge Yang-Mills theory. *Physical Review D*, 101(11), jun 2020.

[34] Boris Lazarevich Ioffe, Victor Sergeevich Fadin, and Lev Nikolaevich Lipatov. *Quantum chromodynamics: Perturbative and nonperturbative aspects.* Cambridge Univ. Press, 2010.

[35] Christian Kellermann and Christian S. Fischer. Running coupling from the four-gluon vertex in Landau gauge Yang-Mills theory. *Physical Review D*, 78(2), jul 2008.

[36] Joseph D. Lykken. Beyond the Standard Model, 2011.

[37] Richard MacKenzie. Path Integral Methods and Applications, 2000.

[38] Michele Maggiore. *A Modern introduction to quantum field theory.* Oxford Master Series in Physics. 2005.

[39] Colin Morningstar. The Monte Carlo method in quantum field theory, 2007.

[40] Herbert Neuberger. Nonperturbative BRS invariance and the Gribov problem. *Physics Letters B*, 183(3):337–340, 1987.

[41] Matthias Neubert. Les Houches Lectures on Renormalization Theory and Effective Field Theories, 2020.

[42] R. Oerter. *The theory of almost everything: The standard model, the unsung triumph of modern physics.* 2006.

[43] Orlando Oliveira and Paulo J. Silva. Lattice Landau gauge gluon propagator: Lattice spacing and volume dependence. *Physical Review D*, 86(11), dec 2012.

[44] Konrad Osterwalder and Robert Schrader. AXIOMS FOR EUCLIDEAN GREEN'S FUNCTIONS. *Commun. Math. Phys.*, 31:83–112, 1973.

[45] Michael E. Peskin and Daniel V. Schroeder. *An Introduction to quantum field theory.* Addison-Wesley, Reading, USA, 1995.

[46] Michael Pippig. PFFT - An extension of FFTW to massively parallel architectures. *SIAM J. Sci. Comput.*, 35, 2013.

[47] Sébastien Rivat. Renormalization Scrutinized. *Studies in History and Philosophy of Science Part B: Studies in History and Philosophy of Modern Physics*, 68:23–39, 2019.

[48] Heinz J. Rothe. *Lattice Gauge Theories : An Introduction (Fourth Edition)*, volume 43. World Scientific Publishing Company, 2012.

[49] L. H. Ryder. *QUANTUM FIELD THEORY.* Cambridge University Press, 6 1996.

[50] H. Sazdjian. Introduction to chiral symmetry in QCD. *EPJ Web of Conferences*, 137:02001, 2017.

[51] Matthew D. Schwartz. *Quantum Field Theory and the Standard Model*. Cambridge University Press, 3 2014.

[52] P.J. Silva and O. Oliveira. Gribov copies, lattice QCD and the gluon propagator. *Nuclear Physics B*, 690(1):177–198, 2004.

[53] A. A. Slavnov. Ward Identities in Gauge Theories. *Theor. Math. Phys.*, 10:99–107, 1972.

[54] J. Smit. *Introduction to quantum fields on a lattice: A robust mate*, volume 15. Cambridge University Press, 1 2011.

[55] H. Sonoda. Wilson's Renormalization Group and Its Applications in Perturbation Theory. *arXiv: High Energy Physics - Theory*, 2006.

[56] George Sterman. Some Basic Concepts of Perturbative QCD, 2008.

[57] Akira Ukawa. Kenneth Wilson and Lattice QCD. *Journal of Statistical Physics*, 160(5):1081–1124, feb 2015.

[58] Milan Vujinovic. Tensor representations of lattice vertices from hypercubic symmetry, 2019.

[59] Milan Vujinović and Tereza Mendes. Probing the tensor structure of lattice three-gluon vertex in Landau gauge. *Physical Review D*, 99(3), feb 2019.

[60] Stefan Weinzierl. Feynman Integrals, 2022.

[61] Peter Weisz. Renormalization and lattice artifacts. *arXiv: High Energy Physics - Lattice*, 2010.

[62] A.G. Williams. QCD, gauge-fixing, and the gribov problem. *Nuclear Physics B - Proceedings Supplements*, 109(1):141–145, may 2002.

[63] Kenneth G. Wilson. Confinement of Quarks. *Phys. Rev. D*, 10:2445–2459, 1974.

[64] D. Zwanziger. Renormalization in the Coulomb gauge and order parameter for confinement in QCD. *Nucl. Phys. B*, 518:237–272, 1998.

A. $SU(N)$ and Colour algebra

$SU(N)$, the special unitary group, is an $(N^2 - 1)$-dimensional group of $N \times N$ unitary matrices with determinant equal to 1. It is a Lie group, so any of its elements can be continuously generated from the identity by the exponential map

$$V \equiv \exp[i\theta^a T_R^a], \tag{A.1}$$

where θ^a are real numbers that parameterize the transformation and T_R^a are the generators in the representation R. The latter are hermitian and traceless matrices that form the Lie algebra, which is the mapping defined by the commutation relation

$$\left[T_R^a, T_R^b\right] = i f^{abc} T_R^c, \tag{A.2}$$

where f^{abc} are real numbers known as the structure constants. In the fundamental representation, these generators are $N \times N$ matrices, and for $N = 3$ they expressed as

$$t^a = \frac{\lambda^a}{2}, \tag{A.3}$$

where λ^a are the 8 Gell-Mann matrices. The generators of the adjoint representation are $(N^2 - 1) \times (N^2 - 1)$ matrices determined by the structure constants,

$$\left(T_{adj}^a\right)^{bc} = -i f^{abc}. \tag{A.4}$$

As seen in section 1.2, for $SU(3)$, the generators of these representations define the gauge field and field-strength tensor, and as such, they will be present in QCD's calculations. Ergo, it is useful to introduce relations between these that facilitate and set conventions for computations involving them, i.e. defining the colour algebra. Here, only the most fundamental relations will be mentioned. See [31] for a more complete review of this subject.

The convention in physics is to define the normalization of the fundamental representation as

$$Tr(t^a t^b) = \frac{1}{2}\delta^{ab}. \tag{A.5}$$

From this, one can write the relation

$$t^a t^b = \frac{1}{2}\left(\frac{\delta^{ab}}{N}I + \left(d^{abc} + i f^{abc}\right) t^c\right), \tag{A.6}$$

where I is the $N \times N$ identity matrix and

$$f^{abc} = -2iTr\left(\left[t^a, t^b\right] t^c\right), \quad d^{abc} = 2Tr\left(\{t^a, t^b\}t^c\right).$$ (A.7)

Finally, these relations enable one to derive

$$f^{abc}f^{abd} = N\delta^{cd}, \quad d^{abc}d^{abd} = \left(\frac{N^2 - 4}{N}\right)\delta^{cd}.$$ (A.8)

Expressions (A.5)-(A.8) are the underlying relations for every calculation performed in this work that involved colour indices, notably the tensor contractions of Chapter 2 and Appendix B.

B. Gluon Vertices Tensor Bases and Form Factors

B.1 Three Gluon Vertex Basis

In the Ball-Chiu construction of the three-gluon vertex basis [7], the Lorentz-space structure reads:

$$\Gamma_{\mu_1\mu_2\mu_3}(p_1, p_2, p_3) = \Gamma^L_{\mu_1\mu_2\mu_3}(p_1, p_2, p_3) + \Gamma^T_{\mu_1\mu_2\mu_3}(p_1, p_2, p_3), \tag{B.1}$$

with

$$\begin{aligned}
\Gamma^T_{\mu_1\mu_2\mu_3}(p_1, p_2, p_3) &= F\left(p_1^2, p_2^2; p_3^2\right)\left(g_{\mu_1\mu_2}p_1 \cdot p_2 - p_{1_{\mu_2}}p_{2_{\mu_1}}\right)B^3_{\mu_3} \\
&+ H\left(p_1^2, p_2^2, p_3^2\right)\left[-g_{\mu_1\mu_2}B^3_{\mu_3} + \frac{1}{3}\left(p_{1_{\mu_3}}p_{2_{\mu_1}}p_{3_{\mu_2}} - p_{1_{\mu_2}}p_{2_{\mu_3}}p_{3_{\mu_1}}\right)\right] \\
&+ \text{cyclic permutations,}
\end{aligned} \tag{B.2}$$

where

$$B^3_{\mu_3} = p_{1_{\mu_3}}p_2 \cdot p_3 - p_{2_{\mu_3}}p_1 \cdot p_2 \tag{B.3}$$

and

$$\begin{aligned}
\Gamma^L_{\mu_1\mu_2\mu_3}(p_1, p_2, p_3) &= A\left(p_1^2, p_2^2; p_3^2\right)g_{\mu_1\mu_2}\left(p_{1_{\mu_3}} - p_{2_{\mu_3}}\right) + B\left(p_1^2, p_2^2; p_3^2\right)g_{\mu_1\mu_2}\left(p_{1_{\mu_3}} + p_{2_{\mu_3}}\right) \\
&+ C\left(p_1^2, p_2^2; p_3^2\right)\left(p_{1_{\mu_2}}p_{2_{\mu_1}} - g_{\mu_1\mu_2}p_1 \cdot p_2\right)(p_1 - p_2)_{\mu_3} \\
&+ \frac{1}{3}S\left(p_1^2, p_2^2; p_3^2\right)\left(p_{1_{\mu_3}}p_{2_{\mu_1}}p_{3_{\mu_2}} + p_{1_{\mu_2}}p_{2_{\mu_3}}p_{3_{\mu_1}}\right) \\
&+ \text{cyclic permutations,}
\end{aligned} \tag{B.4}$$

where the ; notation in the form factors momenta dependence stands for their possible symmetry or anti-symmetry under exchange of the arguments[13].

In the proportional momenta kinematic configuration (2.11), one immediately sees that $\Gamma^T_{\mu_1\mu_2\mu_3} = 0$. The remaining term, $\Gamma^L_{\mu_1\mu_2\mu_3}$, is also seen to vanish in this momenta configuration by taking

---

[13]This ensures that the three gluon vertex, in its Lorentz-colour basis, remains Bose-symmetric. Once more, the reader is pointed to [7].

into account that in the four gluon correlation function decomposition, found in (2.10), we have contractions of the form

$$P^{\mu'_1\mu_1}(p_1)P^{\mu_2\mu'_2}(p_2)\Gamma_{\mu_1\mu_2\mu_3}(p_1,p_2,p_3)P^{\mu_3\mu'_3}(p_3), \tag{B.5}$$

where

$$P^{\mu\mu'}(p) = \left(g^{\mu\mu'} - n\frac{p^\mu p^{\mu'}}{p^2}\right) \tag{B.6}$$

is the momenta-orthogonal projector (2.5), with

$$p_\mu P^{\mu\mu'}(p) = 0 \tag{B.7}$$

and

$$P^{\mu\mu'}(\lambda p) = P^{\mu\mu'}(p). \tag{B.8}$$

From these last two expressions, one directly sees by inspection of (B.4) that we get

$$P^{\mu'_1\mu_1}(p_1)P^{\mu_2\mu'_2}(p_2)\Gamma_{\mu_1\mu_2\mu_3}(p_1,p_2,p_3)P^{\mu_3\mu'_3}(p_3) = 0. \tag{B.9}$$

This leads to the crucial vanishing of the three gluon vertex contribution to the four gluon correlation function (2.10) in our chosen momenta kinematic configuration.

B.2 Four Gluon Vertex Form Factors

Here, we report on the four gluon correlation function and vertex form factors expressions (2.22) and (2.23), for the chosen kinematic configurations (2.24), with the gluon form factors $D(p^2)$ given by (2.6). Note that the following expressions, though derived from the continuum, are computed on the lattice. Hence, $\delta(0) = 1$ and V is the lattice volume, whereas in the continuum, $V = (2\pi)^4$. As stated in Chapter 3, these vacuum expectation values are computed with lattice simulations. Note that in the following, expressions $N = 3$.

$$p_1 = p, \quad p_2 = p, \quad p_3 = p, \quad p_4 = -3p$$

$$\begin{cases} F^{(1)} &= \frac{1}{V}24\langle Tr\left([A_\mu(p),A_\nu(p)]t^r\right)Tr\left([A_\nu(p),A_\mu(-3p)]t^r\right)\rangle \\[2mm] \bar{F}^{(1)} &= \frac{F^{(1)}}{[D(p^2)]^3 D(9p^2)k_{11}} \\[2mm] k_{11} &= P^\mu_\mu(p)P^\nu_\nu(p)P^\eta_\eta(p)P^\zeta_\zeta(p)t^{(1)abcd}_{\mu\nu\eta\zeta}t^{(1)\mu\nu\eta\zeta}_{abcd} = 8748N^2\left(N^2-1\right) \end{cases} \tag{B.10}$$

$$\begin{cases} F^{(2)} &= \frac{1}{V}12\big[\langle Tr\left(A_\mu(p)A_\mu(p)\right)Tr\left(A_\nu(p)A_\nu(-3p)\right)\rangle \\ &\quad +2\langle Tr\left(A_\mu(p)A_\nu(p)\right)Tr\left(A_\mu(p)A_\nu(-3p)\right)\rangle\big] \\[2mm] \bar{F}^{(2)} &= \frac{F^{(2)}}{[D(p^2)]^3 D(9p^2)k_{22}} \\[2mm] k_{22} &= P^\mu_\mu(p)P^\nu_\nu(p)P^\eta_\eta(p)P^\zeta_\zeta(p)t^{(2)abcd}_{\mu\nu\eta\zeta}t^{(2)\mu\nu\eta\zeta}_{abcd} = 157464\left(N^4-1\right) \end{cases} \tag{B.11}$$

$$
\begin{cases}
F^{(3)} &= \frac{1}{\widetilde{\widetilde{k}}_{11}} \widetilde{F}^{(1)} - \frac{1}{k_{11}} F^{(1)} - \frac{\widetilde{\widetilde{k}}_{12}}{k_{22} \widetilde{\widetilde{k}}_{11}} F^{(2)} \\[2ex]
\widetilde{F}^{(1)} &= \frac{1}{V} 24 \langle Tr\left(\{A_\mu(p), A_\nu(p)\} t^r\right) Tr\left(\{A_\nu(p), A_\mu(-3p)\} t^r\right) \rangle \\[2ex]
\widetilde{k}_{11} &= P^\mu_\mu(p) P^\nu_\nu(p) P^\eta_\eta(p) P^\zeta_\zeta(p) \widetilde{t}^{(1)abcd}_{\mu\nu\eta\zeta} t^{(1)\mu\nu\eta\zeta}_{abcd} = -2916N^4 + 14580N^2 - 11664 \\[2ex]
\widetilde{k}_{12} &= P^\mu_\mu(p) P^\nu_\nu(p) P^\eta_\eta(p) P^\zeta_\zeta(p) \widetilde{t}^{(1)abcd}_{\mu\nu\eta\zeta} t^{(2)\mu\nu\eta\zeta}_{abcd} = 69984N^3 - 349920N + \frac{279936}{N} \\[2ex]
\bar{F}^{(3)} &= \frac{F^{(3)}}{[D(p^2)]^3 D(9p^2) k_{33}} \\[2ex]
k_{33} &= P^\mu_\mu(p) P^\nu_\nu(p) P^\eta_\eta(p) P^\zeta_\zeta(p) t^{(3)abcd}_{\mu\nu\eta\zeta} t^{(3)\mu\nu\eta\zeta}_{abcd} = \frac{3}{4N^2(N^2-4)^2(N^2-1)} \big(457019805007872 N^{18} \\
& \quad -4113178245070848 N^{16} + 9597415905165312 N^{14} + 5027217855086592 N^{12} \\
& \quad -544195584 N^{11} - 31534366545543168 N^{10} + 2176782336 N^9 \\
& \quad +9597415905165312 N^8 + 1088391168 N^7 + 32448406155558912 N^6 \\
& \quad -4353564672 N^5 - 17823772395306845 N^4 - 544195584 N^3 \\
& \quad -10968475320188774 N^2 + 2176782336 N + 7312316880125968 \big)
\end{cases}
\tag{B.12}
$$

$$
p_1 = 0, \quad p_2 = p, \quad p_3 = p, \quad p_4 = -2p
$$

$$
\begin{cases}
F^{(1)} &= -\frac{1}{V} 8 \Big[\langle Tr\left([A_\mu(0), A_\nu(p)] t^r\right) Tr\left([A_\mu(p), A_\nu(-2p)] t^r\right) \rangle \\
& \quad - \langle Tr\left([A_\mu(0), A_\nu(p)] t^r\right) Tr\left([A_\nu(p), A_\mu(-2p)] t^r\right) \rangle \\
& \quad + \langle Tr\left([A_\mu(0), A_\nu(-2p)] t^r\right) Tr\left([A_\mu(p), A_\nu(p)] t^r\right) \rangle \Big] \\[2ex]
\bar{F}^{(1)} &= \frac{F^{(1)}}{D(0)[D(p^2)]^2 D(4p^2) k'_{11}} \\[2ex]
k'_{11} &= \frac{4}{3} k_{11}
\end{cases}
\tag{B.13}
$$

39

$$
\begin{cases}
F^{(2)} &= \frac{1}{V}4\big[2\langle Tr\,(A_\mu(0)A_\mu(p))\,Tr\,(A_\nu(p)A_\nu(-2p))\rangle \\
&\quad +2\langle Tr\,(A_\mu(0)A_\nu(p))\,Tr\,(A_\mu(p)A_\nu(-2p))\rangle \\
&\quad +2\langle Tr\,(A_\mu(0)A_\nu(-2p))\,Tr\,(A_\mu(p)A_\nu(p))\rangle \\
&\quad +2\langle Tr\,(A_\mu(0)A_\nu(p))\,Tr\,(A_\nu(p)A_\mu(-2p))\rangle \\
&\quad +\langle Tr\,(A_\mu(0)A_\mu(-2p))\,Tr\,(A_\nu(p)A_\nu(p))\rangle\big] \\[4pt]
\bar{F}^{(2)} &= \dfrac{F^{(2)}}{D(0)[D(p^2)]^2 D(4p^2)k'_{22}} \\[6pt]
k'_{22} &= \frac{4}{3}k_{22}
\end{cases}
\tag{B.14}
$$

$$
\begin{cases}
F^{(3)} &= \dfrac{1}{\widetilde{k}'_{11}}\widetilde{F}^{(1)} - \dfrac{1}{k'_{11}}F^{(1)} - \dfrac{\widetilde{k}'_{12}}{k'_{22}k'_{11}}F^{(2)} \\[8pt]
\widetilde{F}^{(1)} &= \frac{1}{V}8\Big[\langle Tr\,(\{A_\mu(0),A_\nu(p)\}t^r)\,Tr\,(\{A_\mu(p),A_\nu(-2p)\}t^r)\rangle \\
&\quad +\langle Tr\,(\{A_\mu(0),A_\nu(p)\}t^r)\,Tr\,(\{A_\nu(p),A_\mu(-2p)\}t^r)\rangle \\
&\quad +\langle Tr\,(\{A_\mu(0),A_\nu(-2p)\}t^r)\,Tr\,(\{A_\mu(p),A_\nu(p)\}t^r)\rangle\Big] \\[6pt]
\widetilde{k}'_{11} &= \frac{4}{3}k_{11} \\[4pt]
\widetilde{k}'_{12} &= \frac{4}{3}k_{12} \\[4pt]
\bar{F}^{(3)} &= \dfrac{F^{(3)}}{D(0)[D(p^2)]^2 D(4p^2)k'_{33}} \\[6pt]
k'_{33} &= \frac{4}{3}k_{33}
\end{cases}
\tag{B.15}
$$

$$p_1 = 0, \quad p_2 = p, \quad p_3 = 2p, \quad p_4 = -3p$$

$$
\begin{cases}
F^{(1)} &= -\frac{1}{V}4\big[\langle Tr\,([A_\mu(0)A_\nu(p)]t^r)\,Tr\,([A_\mu(2p),A_\nu(-3p)]t^r)\rangle \\
&\quad -\langle Tr\,([A_\mu(0),A_\nu(p)]t^r)\,Tr\,([A_\nu(2p),A_\mu(-3p)]t^r\rangle \\
&\quad +\langle Tr\,([A_\mu(0),A_\nu(2p)]t^r)\,Tr\,([A_\mu(-3p),A_\nu(p)]t^r)\rangle \\
&\quad -\langle Tr\,([A_\mu(0),A_\nu(2p)]t^r)\,Tr\,([A_\nu(-3p),A_\mu(p)]t^r)\rangle \\
&\quad +\langle Tr\,([A_\mu(0),A_\nu(-3p)]t^r)\,Tr\,([A_\mu(p),A_\nu(2p)]t^r)\rangle \\
&\quad -\langle Tr\,([A_\mu(0),A_\nu(-3p)]t^r)\,Tr\,([A_\nu(p),A_\mu(2p)]t^r)\rangle\big] \\[6pt]
\bar{F}^{(1)} &= \dfrac{F^{(1)}}{D(0)D(p^2)D(4p^2)D(9p^2)k'_{11}}
\end{cases}
\tag{B.16}
$$

$$
\begin{cases}
F^{(2)} & = \frac{1}{V}4[\langle Tr\left(A_\mu(0)A_\mu(p)\right)Tr\left(A_\nu(2p)A_\nu(-3p)\right)\rangle \\
& +\langle Tr\left(A_\mu(0)A_\nu(2p)\right)Tr\left(A_\mu(p)A_\nu(-3p)\right)\rangle \\
& +\langle Tr\left(A_\mu(0)A_\nu(-3p)\right)Tr\left(A_\mu(p)A_\nu(2p)\right)\rangle \\
& +\langle Tr\left(A_\mu(0)A_\nu(p)\right)Tr\left(A_\mu(2p)A_\nu(-3p)\right)\rangle \\
& +\langle Tr\left(A_\mu(0)A_\mu(2p)\right)Tr\left(A_\nu(p)A_\nu(-3p)\right)\rangle \\
& +\langle Tr\left(A_\mu(0)A_\nu(-3p)\right)Tr\left(A_\nu(p)A_\mu(2p)\right)\rangle \\
& +\langle Tr\left(A_\mu(0)A_\nu(p)\right)Tr\left(A_\nu(2p)A_\mu(-3p)\right)\rangle \\
& +\langle Tr\left(A_\mu(0)A_\nu(2p)\right)Tr\left(A_\nu(p)A_\mu(-3p)\right)\rangle \\
& +\langle Tr\left(A_\mu(0)A_\mu(-3p)\right)Tr\left(A_\nu(p)A_\nu(2p)\right)\rangle] \\
\\
\bar{F}^{(2)} & = \frac{F^{(2)}}{D(0)D(p^2)D(4p^2)D(9p^2)k'_{22}}
\end{cases}
\tag{B.17}
$$

$$
\begin{cases}
F^{(3)} & = \frac{1}{\widetilde{k}'_{11}}\widetilde{F}^{(1)} - \frac{1}{k'_{11}}F^{(1)} - \frac{\widetilde{k}'_{12}}{k'_{22}\widetilde{k}'_{11}}F^{(2)} \\
\\
\widetilde{F}^{(1)} & = \frac{1}{V}4\Big[\langle Tr\left(\{A_\mu(0)A_\nu(p)\}t^r\right)Tr\left(\{A_\mu(2p),A_\nu(-3p)\}t^r\right)\rangle \\
& +\langle Tr\left(\{A_\mu(0),A_\nu(p)]t^r\right)Tr\left([\{A_\nu(2p),A_\mu(-3p)\}t^r\rangle \\
& +\langle Tr\left(\{A_\mu(0),A_\nu(2p)]t^r\right)Tr\left(\{A_\mu(-3p),A_\nu(p)\}t^r\right)\rangle \\
& +\langle Tr\left(\{A_\mu(0),A_\nu(2p)]t^r\right)Tr\left(\{A_\nu(-3p),A_\mu(p)\}t^r\right)\rangle \\
& +\langle Tr\left(\{A_\mu(0),A_\nu(-3p)]t^r\right)Tr\left(\{A_\mu(p),A_\nu(2p)\}t^r\right)\rangle \\
& +\langle Tr\left(\{A_\mu(0),A_\nu(-3p)]t^r\right)Tr\left(\{A_\nu(p),A_\mu(2p)\}t^r\right)\rangle\Big] \\
\\
\bar{F}^{(3)} & = \frac{F^{(3)}}{D(0)D(p^2)D(4p^2)D(9p^2)k'_{33}}
\end{cases}
\tag{B.18}
$$

C. Additional Results

This Appendix provides additional data that was used in the computation of the four gluon vertex in a volume of 32^4 lattice points and averaged over an ensemble of 4620 configurations.

C.1   Gluon Propagators

The gluon propagator form factor data was used to compute the four gluon vertex form factors (2.23) and are therefore given here. These are computed from the expression (2.6), with its lattice version being the ensemble average

$$D(p^2) = \frac{\langle Tr\left[A_\mu(p_1)A_\mu(p_2)\right]\rangle}{V\left(16 - 4n\right)}. \tag{C.1}$$

Note that the gluon propagator form factors statistical errors were considered when plotting this data, despite not being visible due to their small values.
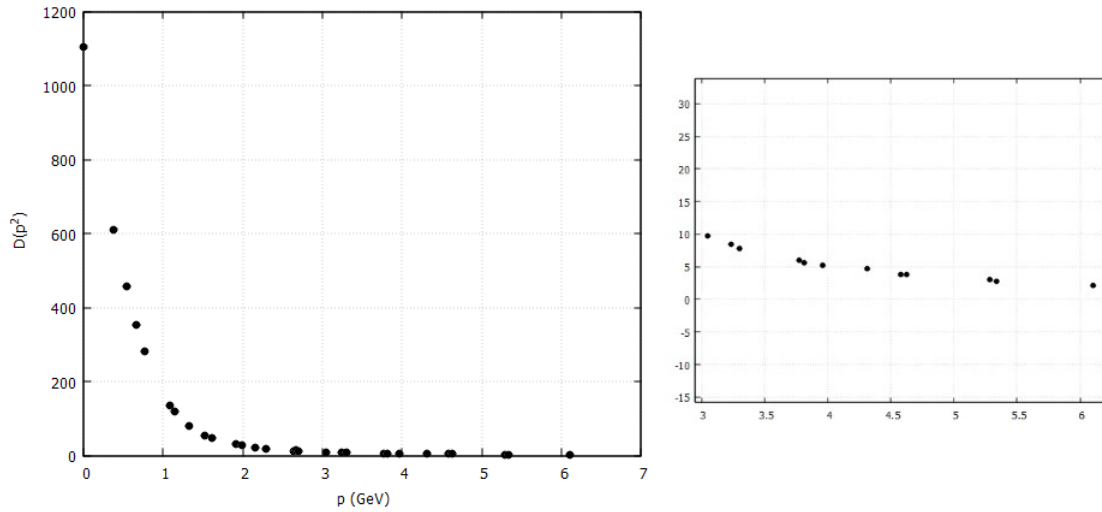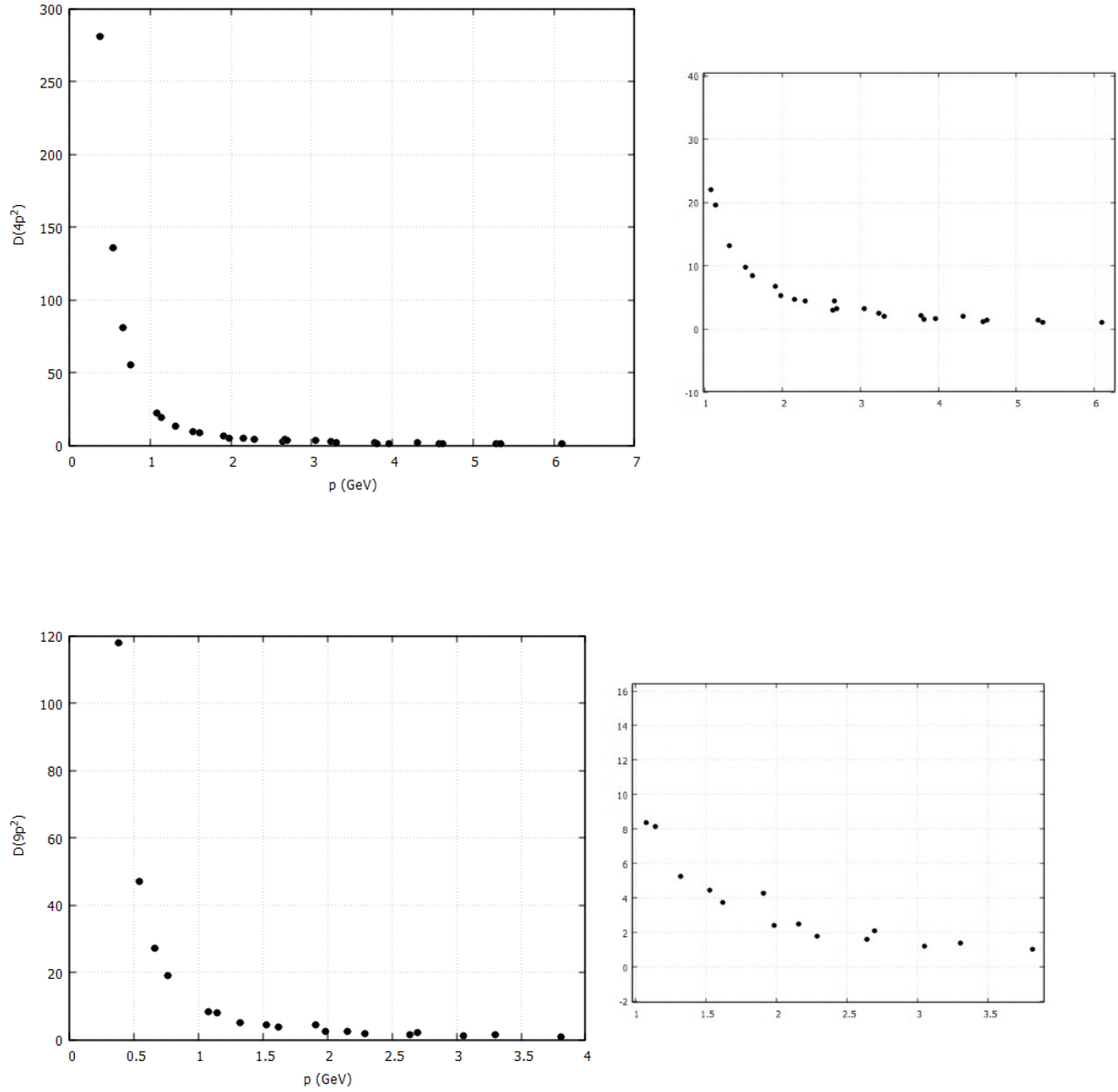
Figure C.1: The bare gluon propagator form factors $D(p^2)$, $D(4p^2)$ and $D(9p^2)$, computed on a lattice of volume 32^4. The plot on the left contains all the computed data, whilst the plot on the right is a zoom-in of the left plot.

C.2   Full Results for the Four Gluon Correlation Function Form Factors

Most of the computed data of the four gluon correlation function form factors was omitted in Chapter 4 due to momentum-space cut and form factor average due to their $H(4)$ invariants dependence. Here, the ensemble average of all the lattice extracted data is presented, showing the lack of signal-to-noise ratio that led to the momentum-space cuts.
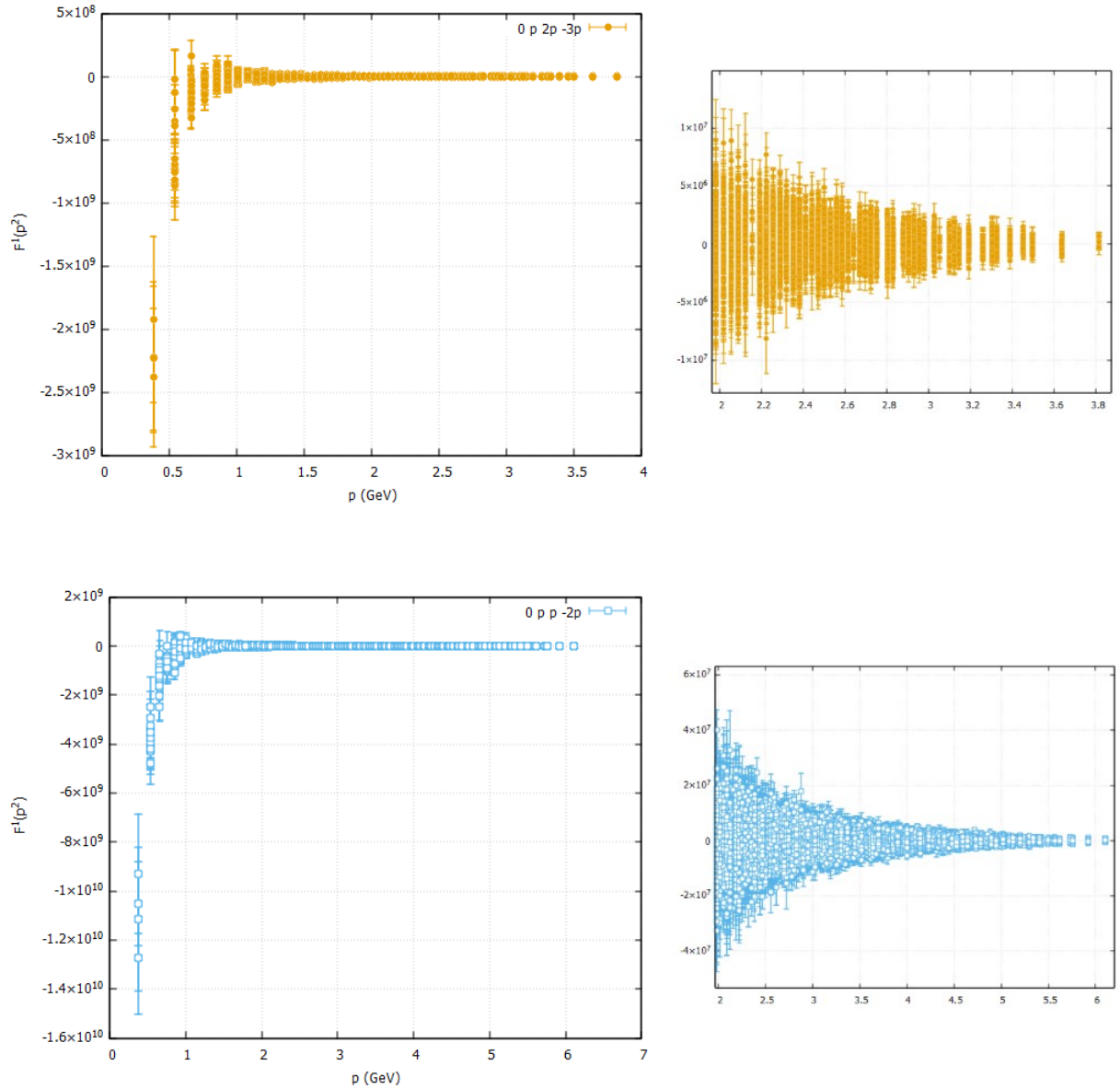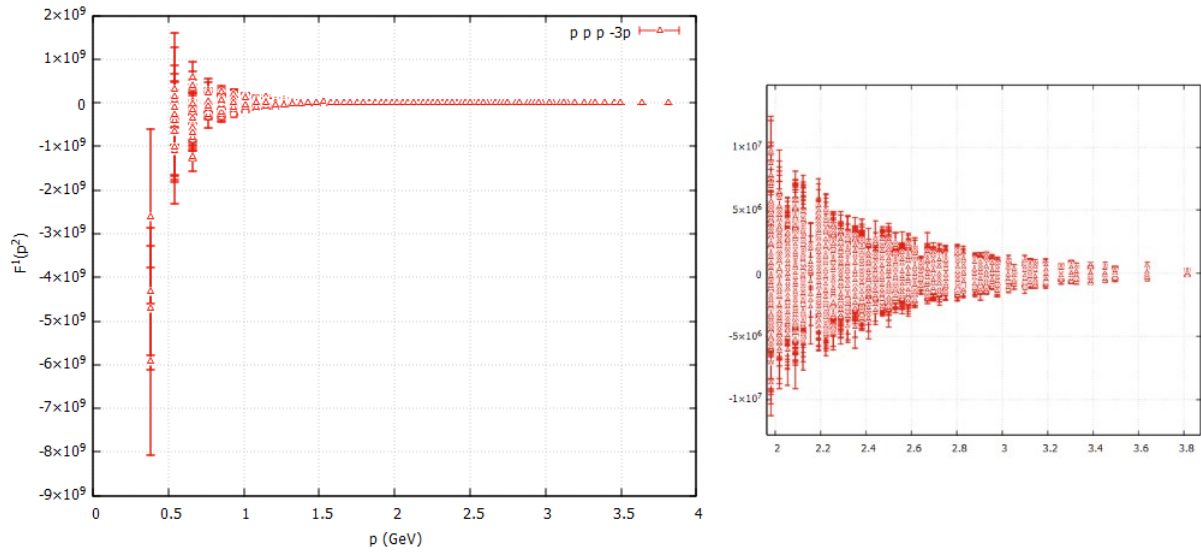
Figure C.2: The bare $F^1(p^2)$ form factor data for the kinematic configurations used in this work, computed on a lattice of volume 32^4. The plot on the left contains all the computed data, whilst the plot on the right is a zoomed-in of the left plot.
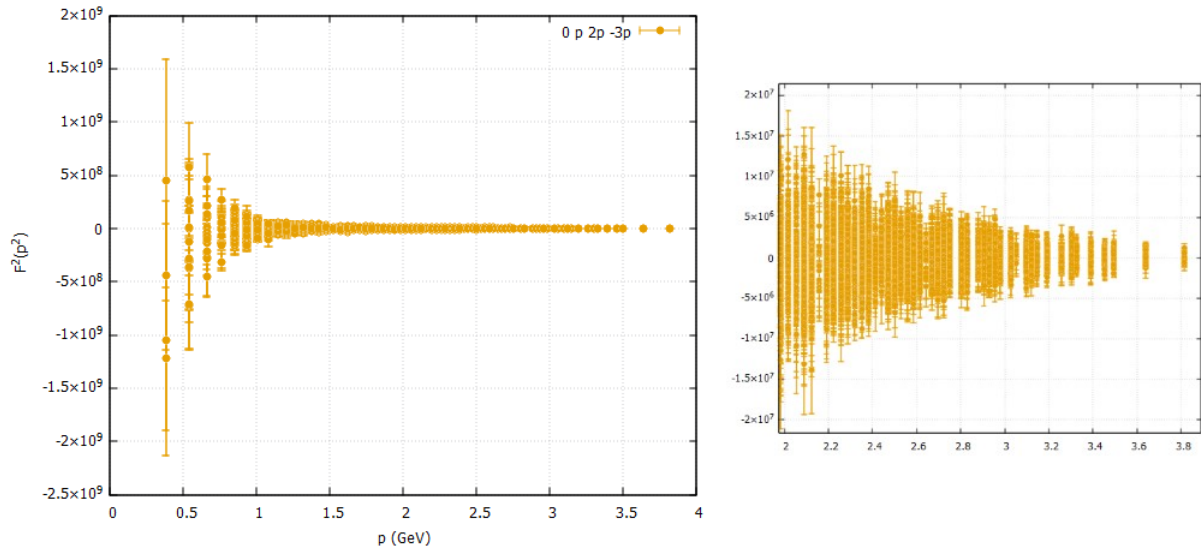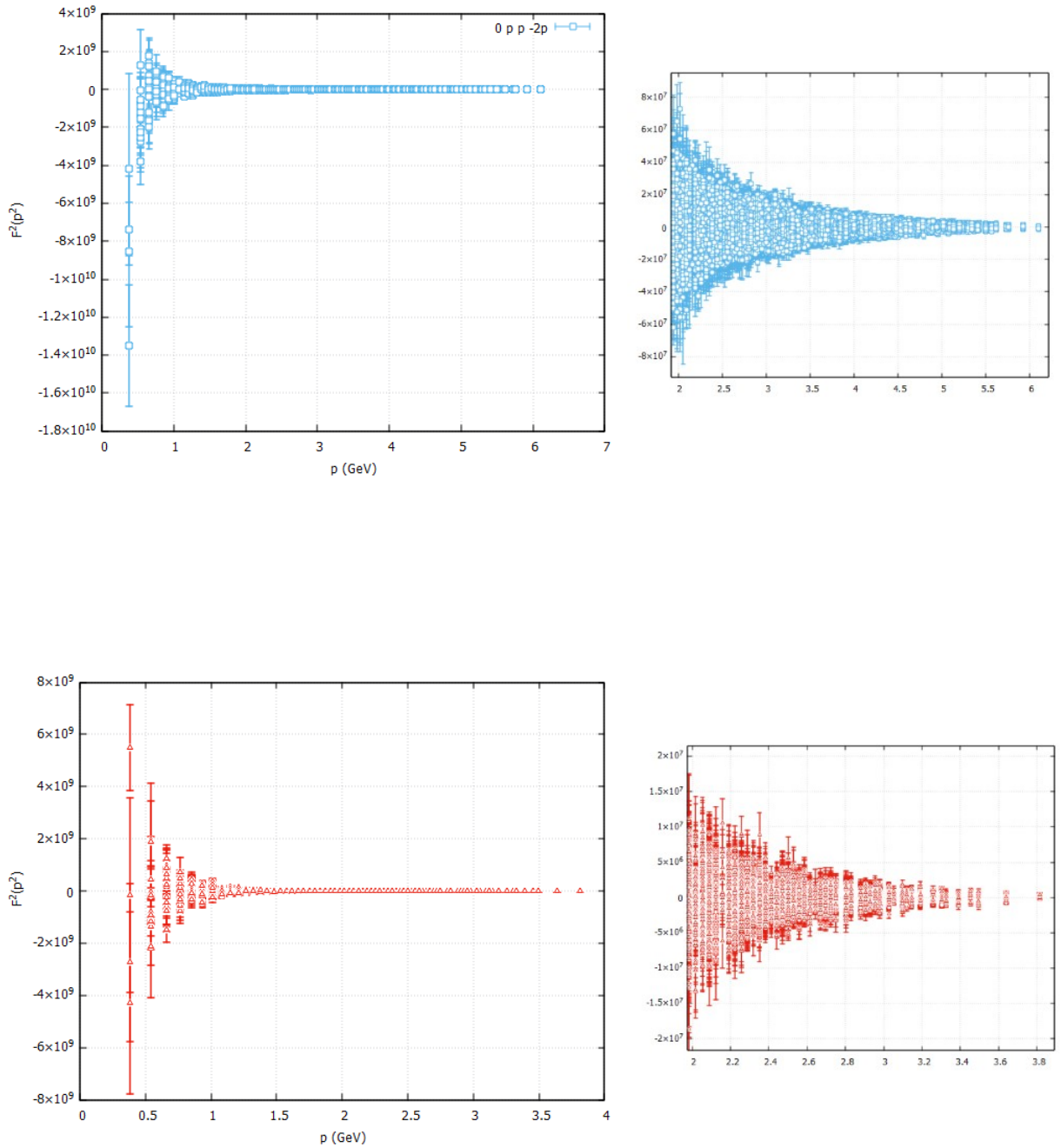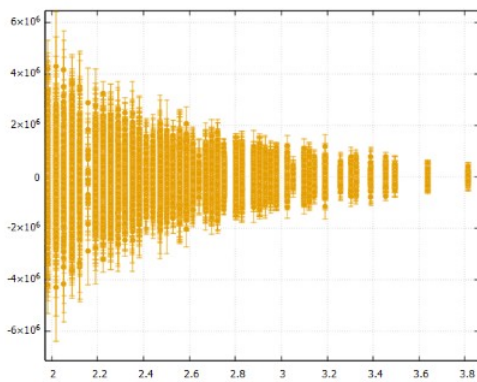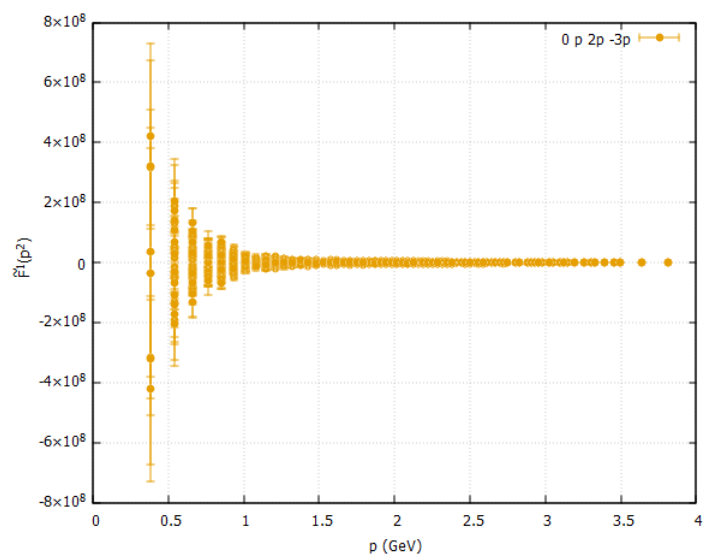
Figure C.3: The bare $F^2(p^2)$ form factor data for the kinematic configurations used in this work, computed on a lattice of volume 32^4. The plot on the left contains all the computed data, whilst the plot on the right is a zoom-in of the left plot.
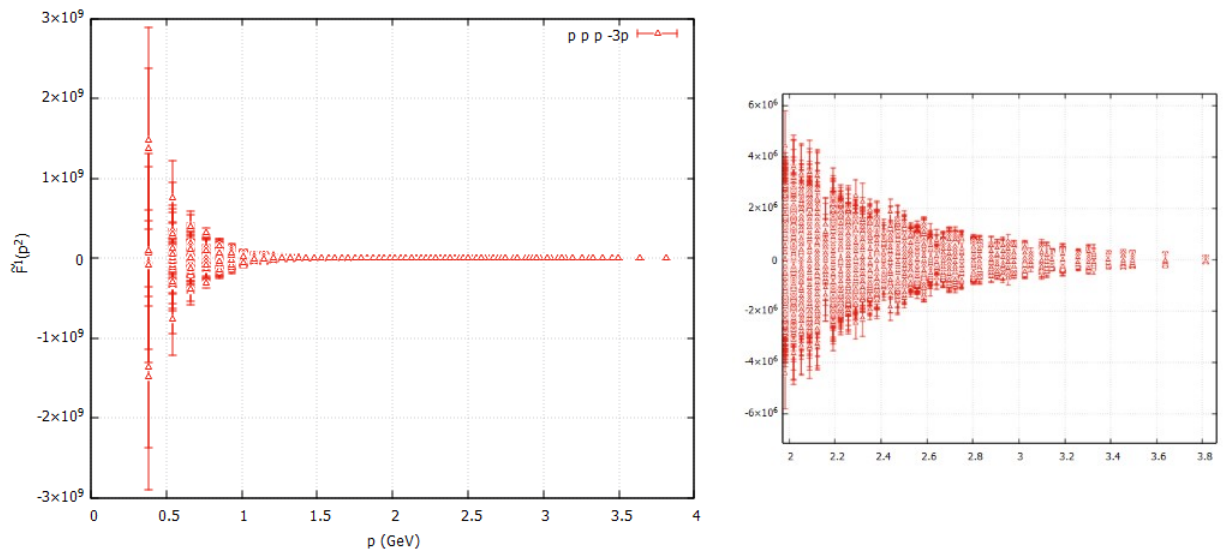
47
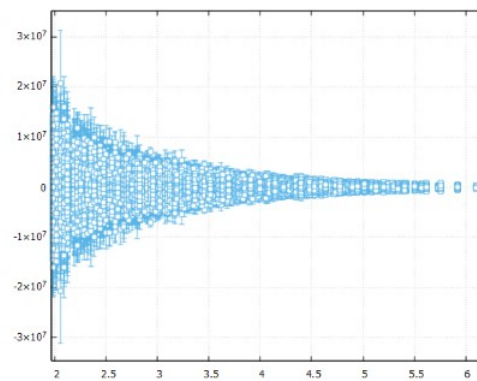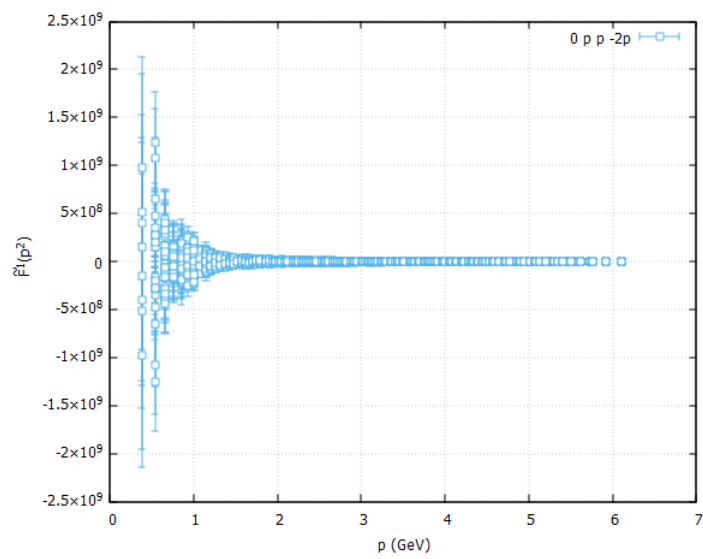
Figure C.4: The bare $\tilde{F}^1(p^2)$ form factor data for the kinematic configurations used in this work, computed on a lattice of volume 32^4. The plot on the left contains all the computed data, whilst the plot on the right is a zoom-in of the left plot.